



HAL
open science

Metallome deregulation and health-related impacts due to long-term exposure to recent volcanic ash deposits: New chemical and isotopic insights

Lucie Sauzéat, Julia Eychenne, Lucia Gurioli, Maud Boyet, David Jessop, Roberto Moretti, Mélusine Monrose, Hélène Holota, Claude Beaudoin, David Volle

► To cite this version:

Lucie Sauzéat, Julia Eychenne, Lucia Gurioli, Maud Boyet, David Jessop, et al.. Metallome deregulation and health-related impacts due to long-term exposure to recent volcanic ash deposits: New chemical and isotopic insights. *Science of the Total Environment*, In press, 829, pp.154383. 10.1016/j.scitotenv.2022.154383 . hal-03610668

HAL Id: hal-03610668

<https://uca.hal.science/hal-03610668v1>

Submitted on 16 Mar 2022

HAL is a multi-disciplinary open access archive for the deposit and dissemination of scientific research documents, whether they are published or not. The documents may come from teaching and research institutions in France or abroad, or from public or private research centers.

L'archive ouverte pluridisciplinaire **HAL**, est destinée au dépôt et à la diffusion de documents scientifiques de niveau recherche, publiés ou non, émanant des établissements d'enseignement et de recherche français ou étrangers, des laboratoires publics ou privés.



Distributed under a Creative Commons Attribution - NonCommercial - NoDerivatives 4.0 International License

Science of the Total Environment

Metallome deregulation and health-related impacts due to long-term exposure to recent volcanic ash deposits: new chemical and isotopic insights

--Manuscript Draft--

Manuscript Number:	STOTEN-D-21-29496R1
Article Type:	Research Paper
Section/Category:	
Keywords:	volcanic ash deposits, La Soufrière de Guadeloupe volcano, metallome, Cu-Zn isotopes, in-vivo assays
Corresponding Author:	Lucie Sauzeat Laboratoire Magmas et Volcans Aubièrre Cedex, FRANCE
First Author:	Lucie Sauzeat
Order of Authors:	Lucie Sauzeat Julia Eychenne Lucia Gurioli Maud Boyet David E. Jessop Roberto Moretti Mélusine Monrose Hélène Holota Claude Beaudoin David H. Volle
Abstract:	<p>Volcanic ash exposure can lead to significant health risks. Damage to the respiratory and pulmonary systems are the most evident toxic side effects although the causes of these symptoms remain unclear. Conversely, the effects on other organs remain largely under-explored, limiting our understanding of the long-term volcanic ash-related risk at the whole-body scale. The metallome i.e. metal concentrations and isotopic compositions within the body, is suspected to be affected by volcanic ash exposure, having thus the potential for capturing some specificities of ash toxicity. However, the means by and extent to which the metallome is affected at the entire body scale and how the consequent chemical and isotopic deregulations correlate with pathophysiological dysfunctions are currently poorly understood. Here, we adopt a transdisciplinary approach combining high precision chemical analyses (major and trace element concentrations) and Cu-Zn isotope measurements in seven organs and two biological fluids of isogenic mice (C57BL/6) exposed to eruption products from La Soufrière de Guadeloupe (Eastern Caribbean), in tandem with biological parameters including physiological and morphological data. Based on principal component analysis, we show that after one month of exposure to volcanic ash deposits, the mice metallome; originally organ-specific and isotopically-typified, is highly disrupted as shown for example by heavy metal accumulation in testis (e.g., Fe, Zn) and Cu, Zn isotopic divergence in liver, intestine and blood. These metallomic variations are correlated with early testicular defects and might reflect the warning signs of premature (entero)hepatic impairments that may seriously affect fertility and favor the emergence of liver diseases after prolonged exposure. Monitoring the temporal evolution of the Cu and Zn isotope compositions seems to be a promising technique to identify the main biological processes and vital functions that are vulnerable to environmental volcanogenic pollutants although this will require further validation on human subjects.</p>
Response to Reviewers:	Ms. Ref. No.: STOTEN-D-21-29496 Title: Metallome deregulation and health-related impacts due to long-term volcanic ash exposure: new chemical and isotopic insights from la Soufrière de Guadeloupe volcano



Highlights

- Volcanic ash is a major metal-rich contaminant
- Chronic exposure to volcanic ash results into an organ-specific and isotopically-typified metallome deregulation
- Mice metallome deregulations are associated to severe pathophysiological changes
- Quantification of copper and zinc isotopic compositions may appear as an innovative technique to diagnose volcanic-related pathophysiological dysfunctions

1 **Metallome deregulation and health-related impacts due to long-term exposure to recent** 2 **volcanic ash deposits: new chemical and isotopic insights**

3
4 Lucie Sauzéat^{1,2}, Julia Eychenne^{1,2}, Lucia Gurioli^{1,3,4}, Maud Boyet¹, David Jessop^{1,3,4}, Roberto
5 Moretti^{3,4}, Mélusine Monroe², Hélène Holota², Claude Beaudoin², David H. Volle²

6
7 ¹ Université Clermont Auvergne, CNRS, IRD, OPGC, Laboratoire Magmas et Volcans, F-
8 63000 Clermont-Ferrand, France

9 ² Université Clermont Auvergne, CNRS UMR 6293, Inserm U1103, Génétique, Reproduction
10 et Développement, F-63000 Clermont-Ferrand, France

11 ³ Université de Paris, Institut de physique du globe de Paris, CNRS UMR 7154, F-75005 Paris,
12 France

13 ⁴ Observatoire volcanologique et sismologique de Guadeloupe, Institut de physique du globe
14 de Paris, F-97113 Gourbeyre, France

15 Corresponding Author: Lucie Sauzéat / mail: lucie.sauzeat@uca.fr

16 17 **Abstract**

18 Volcanic ash exposure can lead to significant health risks. Damage to the respiratory and
19 pulmonary systems are the most evident toxic side effects although the causes of these
20 symptoms remain unclear. Conversely, the effects on other organs remain largely under-
21 explored, limiting our understanding of the long-term volcanic ash-related risk at the whole-
22 body scale. The metallome *i.e.* metal concentrations and isotopic compositions within the body,
23 is suspected to be affected by volcanic ash exposure, having thus the potential for capturing
24 some specificities of ash toxicity. However, the means by and extent to which the metallome
25 is affected at the entire body scale and how the consequent chemical and isotopic
26 deregulations correlate with pathophysiological dysfunctions are currently poorly understood.
27 Here, we adopt a transdisciplinary approach combining high precision chemical analyses
28 (major and trace element concentrations) and Cu-Zn isotope measurements in seven organs
29 and two biological fluids of isogenic mice (C57BL/6) exposed to eruption products from La
30 Soufrière de Guadeloupe (Eastern Caribbean), in tandem with biological parameters including
31 physiological and morphological data. Based on principal component analysis, we show that
32 after one month of exposure to volcanic ash deposits, the mice metallome; originally organ-
33 specific and isotopically-typified, is highly disrupted as shown for example by heavy metal
34 accumulation in testis (*e.g.*, Fe, Zn) and Cu, Zn isotopic divergence in liver, intestine and blood.
35 These metallomic variations are correlated with early testicular defects and might reflect the
36 warning signs of premature (entero)hepatic impairments that may seriously affect fertility and
37 favor the emergence of liver diseases after prolonged exposure. Monitoring the temporal
38 evolution of the Cu and Zn isotope compositions seems to be a promising technique to identify
39 the main biological processes and vital functions that are vulnerable to environmental
40 volcanogenic pollutants although this will require further validation on human subjects.

41 **Keywords:** volcanic ash deposits, La Soufrière de Guadeloupe volcano, metallome, Cu-Zn
42 isotopes, *in-vivo* assays

43 44 45 **1. Introduction**

46 Covering approximately 124 million hectares of the world's land surface¹, volcanic ash soils
47 are home to more than 8 million people². By definition, volcanic ash soils designate soils
48 formed from volcanoclastic materials including ash³ (defined as small fragments of quenched
49 magma and eroded substratum smaller than 2 mm in diameter). Such soils are regularly
50 formed, given that every month, active volcanoes release more than a million cubic meters of
51 volcanic ash into Earth's atmosphere⁴. Upon injection, ash undergoes several physicochemical
52 processes including interactions with gas, aerosols and anthropogenic pollutants compounds
53 that may affect its surface composition and reactivity^{5,6}. These volcanic particles are then

54 deposited within minutes to years on the ground followed by wind- and water-driven erosion,
55 long-term stabilization, consolidation and finally pedogenesis processes accounting for
56 volcanic soil formation^{3,5}. The intensity of wind erosion and the subsequent resuspension of
57 deposited volcanic ash, which can be a dominant feature of a post-eruptive landscape⁵,
58 coupled with intense human activities may result in long-term human exposure to these soil
59 particles. Particle absorption can occur by several exposure pathways, including inhalation as
60 well as oral and dermal uptake and thus represent a major health issue. So far, only a few
61 biological studies using animal models focused on the impact of acute exposure to ultra-fine
62 volcanic particles (<10 µm) either by inhalation or intratracheal injection over short periods of
63 time^{7,8,9}. These studies demonstrate that short-term intense volcanic ash exposure induces
64 adverse effects on the respiratory tracts^{7,9}. Biological studies on pulmonary cell models also
65 point towards acute inflammatory reaction¹⁰⁻¹². In parallel, several epidemiological studies
66 show higher incidences of respiratory diseases such as chronic bronchitis¹³ in some volcanic
67 areas affected by volcanic ash fallout, as well as other pathologies like multiple sclerosis¹⁴,
68 thyroid¹⁵ and gastrointestinal cancers¹⁶ in populations living daily in a volcanic environment.
69 This may suggest a more global and longer-term relationship, likely resulting from multiple
70 uptake routes not limited to inhalation, between volcanogenic contaminants exposure,
71 including volcanic ash, and health impairments, although this remains to be proven. Another
72 important point relies on the toxicity parameters, as the nature and the intensity of the
73 symptoms may depend on the physico-chemical properties of the volcanic particles. Studies
74 have shown that cristobalite, a crystalline silica phase, was a main component of volcanic ash
75 inducing inflammation¹¹; crystalline silica being also known for triggering silicosis¹⁷, a type of
76 pulmonary fibrosis. However, crystalline silica is not the only toxic compound present in
77 volcanic deposits as metals, such as copper (Cu), zinc (Zn) and iron (Fe), may also contribute
78 to volcanic particles' toxicity. So far, only few studies have focused on these trace
79 elements^{15,18}, with a specific focus on chemical concentrations to the detriment of stable
80 isotopic compositions, but none of them has never quantified the whole-body metallome
81 deregulations at the entire body-scale following chronic exposure. The term metallome refers
82 here to the entirety of metal- and metalloid species present in a biological system, defined as
83 to their identity (e.g. isotopic form) and/or quantity (concentration) (for a complete definition
84 see Lobinski et al.¹⁹). Recently recognized as very promising tools in the medical field, stable
85 metal isotope analyses have contributed to the development of new research perspectives to
86 better understand the complexity, causes and underlying mechanisms of aging^{20,21} and many
87 severe diseases such as cancers²² and neurodegenerative disorders²³.

88 Firstly, the present study aims at elucidating whether long-term exposure to recently ground-
89 deposited volcanic ash (a proxy of premature volcanic soils i.e. early stage of pedogenesis) by
90 various and simultaneous exposure routes (inhalation, oral and dermal) contribute to
91 widespread metallome deregulations related to severe pathological disorders at the entire
92 body-scale. Secondly, this project focus at determining to what extent stable isotopes may help
93 to better characterize the toxic and potentially carcinogenic effect of ash-derived metals in a
94 volcanically active area. We report on the metallome of seven organs and two body fluids
95 (blood and urine) in tandem with a series of physio-, immuno- and morphological data collected
96 on mice exposed to bulk "volcanic ash-made" from La Soufrière de Guadeloupe volcano
97 (hereby referred to as "La Soufrière"). La Soufrière is an explosive-type active volcano located
98 in the Lesser Antilles arc that has experienced many magmatic and phreatic eruptions in the
99 past. The last 1976-1977 phreatic eruptive crisis was characterized by important steam blasts
100 that gave rise to particle and sometimes block-charged plumes resulting in the deposition of
101 10⁶ m³ of volcanic ash and blocks on the ground²⁴. After that, a regular decrease in the activity
102 of La Soufrière was observed until the beginning of the 1990s. Since 1992, the volcanic and
103 seismic activity shows a gradual increase that reached a record level on 27 April 2018 with the
104 largest volcano-tectonic earthquake (M_L 4.1) associated to an intense hydrothermal and
105 fumarolic activity²⁵. This event, regarded as a failed phreatic eruption²⁵, marked a significant
106 change of the volcano regime that may foreshadow the onset of an upcoming series of phreatic
107 and magmatic eruptions, resulting in large volcanic ash fallout. The current level of volcanic
108 activity includes regular swarms of volcano-tectonic earthquakes, active degassing from a

109 number of high-flux fumarole vents, and a spreading and intensification of ground thermal
110 anomalies at the summit^{26,27}. These signs indicate that the ongoing unrest may escalate
111 towards more explosive activity (either phreatic or magmatic) in the future, meaning that
112 studies on the health impacts of volcanic emissions at La Soufrière are highly worthwhile due
113 to the major population zones (~20 000 people within 10 km of the volcano). Furthermore, as
114 La Soufrière is a close analogue for numerous other andesitic to dacitic “arc” volcanoes (i.e.
115 with a similar rock composition^{28,29}) worldwide, such studies are of great importance for our
116 understanding of the health impacts of volcanoes on human and other organisms.
117

118 **2. Materials and methods**

119 **2.1. Geological field sampling and sample preparation**

120 Because recently ground-deposited fresh volcanic ash was not available at La Soufrière, a
121 laboratory-crushed volcanic ash was produced. The aim was to simulate, within uncertainties
122 of experimental protocols, a proxy of premature volcanic soils. Volcanic ash can be generated
123 by the fragmentation of rocks present on the volcanic edifice, especially during dome-collapse
124 explosive eruptions. We thus collected four volcanic blocks (S01-S04) from the most recent
125 lava dome (emplaced during the AD 1530 eruption³⁰) at two active sites that are the “Tarissan”
126 and the “Cratère Sud” (Figure 1; see Supp. Table 1 for GPS coordinates). These blocks,
127 exhibiting a pronounced surface alteration but well-preserved internal facies (Supp. Figure 1a),
128 were crushed using a Jaw crusher BB 250 (Retsh Company) heavy-metal free steel grinding
129 tool before being separated in different size fractions at half-phi size intervals (where $\Phi = -$
130 \log_2 [particle diameter in mm]), using stainless-steel sieves (SAULAS brand). Particle grain size
131 analyses were performed on the size fraction finer than 63 μ m using the laser diffraction
132 technique (Malvern Mastersizer®). Defined amounts of each fraction were then mixed together
133 to reproduce a realistic particle size distribution for volcanic ash (i.e., mirroring the average
134 grain size of volcanic particles commonly produced by explosive eruptions³¹), with a median
135 grain size of about 100 μ m (3.5 Φ) (Supp. Figure 1b). The fraction above 2 mm (-1 Φ) was
136 excluded, volcanic ash being defined as volcanic particles <2 mm (<-1 Φ) in size.
137
138

139 **2.2. Mice *in-vivo* assays**

140 **2.2.1. Ethics statement**

141 In this study, all the animal experiments comply with the ARRIVE and the EU Directive 2010/63
142 guidelines and were conducted in accordance with the current regulations and standards
143 approved by the Animal Care Committee (APAFIS #33604).
144

145 **2.2.2. Exposure protocol**

146 Because of their genetic, physiological and metallomic regulation processes homologies with
147 humans^{32,33}, mice have long served as models of human biology and provide, so far, the
148 foremost mammalian model for studying human diseases and more broadly human health.
149 Male C57BL/6 mice (5-month-old) were purchased from Charles River Laboratories and
150 maintained under 12-hour light/dark cycles, in controlled temperature, pressure and
151 atmospheric (22°C, humidity <50%) cages (500 cm² EasyCage® - Allentown; three mice per
152 cage). To mimic chronic exposure, mice were exposed to volcanic ash over a month. C57BL/6
153 mice have a median lifespan ranging between 27 to 29 months, equivalent to a human lifespan
154 of 80-84 years. By analogy, one month on a mouse scale will thus correspond to about 3 years
155 of persistent exposure for a human. All the cages were previously filled with 100 g of corn cob
156 litter (NestPak®) for the control group (n=6) or a mixture of corn cob litter (NestPak®) and
157 volcanic ash (200 g of litter for 100 g of ash) for the exposed group (n=6). To ensure breathable
158 air, cages were supported by EcoFlo™ ventilated rack mounted blowers with a total air volume
159 renewed 50 times per hour. Over the time exposure, mice had *ad libitum* access to food
160 (Teklad Global Rodent Diet®, Envigo+++) and water. The chemical composition of the diet is
161 given in Supp. Table 2. Body weight as well as food and water intake were measured three
162 times per week to establish growth curves and estimate daily food (g/day/mouse) and water
163 (mL/day/mouse) consumption (Supp. Table 3 and Supp. Figure 2).

164
165
166
167
168
169
170
171
172
173
174
175
176
177
178
179
180
181
182
183
184
185
186
187
188
189
190
191
192
193
194
195
196
197
198
199
200
201
202
203
204
205
206
207
208
209
210
211
212
213
214
215
216
217
218

2.3. Biological samples collection, preparation and measurements

2.3.1. Sample collection & preparation

After one month of exposure, urine was first collected in acid-cleaned Eppendorf tubes®. To ensure sufficient volume for precise chemical and isotopic measurements, the urine of the mice present in the same cage were pooled. All mice were then sacrificed by decapitation and organ dissection was performed with acid-clean scissors and vinyl gloves to ensure minimal metal exogenous contamination. Chemical (e.g., pentobarbital) and inhalant gas (e.g., isoflurane, CO₂) anesthetics, commonly used to euthanize the mice as well as some type of gloves may contain elevated amounts of metals that can significantly bias the chemical and isotopic results³⁴. Decapitation is thus the most suitable alternative technique with regard to its lowest chemical contamination effect. Like for urine, blood was collected into acid-clean Eppendorf tubes®, taking care not to use plastic syringes and traditional collection tubes like heparinized or rubber-stoppered evacuated tubes that may give rise to significant and artificial increase of blood, plasma and serum metal contents up to 250%^{35,36}. For the organs, we collected liver, brain, lung, kidney, intestine, testis and heart. Each of them was then weighed (Supp. Table 4). Entire organ for brain, heart, intestine and half organ for liver, kidney, testis and lung were then freeze-dried for 48h (Christ Alpha™ Freeze dryer 1-2 LD+). All samples were stored at -80°C until further chemical processing.

2.3.2. Histology & Sperm counts

For liver, kidney, testis and lung, the remaining part was paraformaldehyde (PFA)-fixed for 48h and embedded in paraffin. Five µm thick sections were then prepared and stained with Hematoxylin/Eosin (HE) and Masson's Trichrome (TM) for histological analysis using a Zeiss Axioscan Microscope Slide Scanner. For testes, epididymal sperm counts and quantification of the epithelium thickness (R_{epi}), defined as the ratio between the total (D_t) and the inner diameter (D_i) of the seminiferous tubules, were also performed. All data are reported in Supp. Tables 5 and 6 respectively. To avoid any analytical bias, all these analyses were performed only in rounded tubules ($n > 20$ per sample). For sperm counts, the tail and the head of the epididymis were disrupted and placed in phosphate buffered saline (PBS) solution to ensure spermatozoa remobilization and three independent sperm count ($\times 10^6$, $n=3$) were assessed using a Malassez slide (20-fold and 100-fold dilution for tail and head of epididymis respectively).

2.3.3. Immunohistochemistry

Testicular immunohistological analyses were conducted according to the manufacturer's recommendations. Briefly, 5 µm sections were mounted on positively charged glass slides (Superfrost plus) before being deparaffinized, rehydrated, treated for 20 min at 93–98 °C in 0.01 M citric buffer–Tween 0.1% (pH 6), rinsed in osmosed water (2 x 5 min), and washed (2 x 5 min) in phosphate-buffered saline (PBS). Thin sections were then incubated in blocking solutions (PBS 1x + 10% FBS-fetal bovine serum) for 1h at room temperature. Primary SOX9 (Millipore, AB5535), SYCP3 (Abcam, 97672), PLZF (Santa Cruz, SC-28319) and acetyl-Histone H4 (H4ac, Millipore, 06-946) antibodies were then diluted in blocking solution and applied to samples overnight at 4°C. After several washes in PBS 1x, a first step of polymeric amplification with HRP (horse-radish polymerase) were performed for 30 min at room temperature (only for SYCP3 and PLZF antibodies). Fluorophore-conjugated secondary antibodies were then applied for 1h at room temperature. After several washes in PBS 1x, the slides were then counterstained with Hoechst medium (1 mg/mL) (Invitrogen, Cergy Pontoise, France), mounted on PBS/glycerol (50 % v/v) and imaged with a Zeiss Axioscan Microscope Slide Scanner. Immunohistochemical quantification were then performed on the open source QuPath software to count the proportion of normal seminiferous tubules. This proportion was estimated by counting (i) the number of PLZF and SOX9 positive cells per seminiferous tubules and (ii) the number of seminiferous tubules with H4ac. and SYCP3 positive cells normalized to the total number of tubules. For each section, all the rounded seminiferous tubules were counted ($n > 20$). All the data are reported in Supp. Table 6.

219 **2.4. Major and trace elements**

220 All chemical analyses were carried out in clean laminar flow hoods using double-distilled acids
221 to avoid any exogenous contaminations.

222 All the biological samples including freeze-dried organs, blood, urine and mice food, were
223 dissolved in a concentrated HNO₃-H₂O₂ mixture in Savillex beakers at 100°C for at least 72 h.
224 After complete digestion, major and trace element concentrations were measured in a small
225 aliquot on an ICP-AES (Agilent 5800) and a quadrupole ICP-MS (Agilent 7500), respectively,
226 at the Laboratoire Magmas et Volcans (LMV) following the method described in Garçon et
227 al.,³⁴. When necessary, analytical drift was corrected using indium (In) addition as internal
228 standard for trace elements. The validity and reproducibility of major and trace element
229 concentrations are estimated to be around 5% (2sd) based on re-run analysis (bis) and
230 complete duplicates of international (*i.e.*, bovine liver, 1577c) biological reference material (see
231 Supp. Table 2). Major and trace element concentrations are all reported in µg/g (ppm) and
232 ng/g (ppb) dry weight respectively in Supp. Table 2.

233 For geological samples, before any measurements, volcanic ash was further ground in an
234 agate mortar to ensure homogeneity. Major and trace concentrations were then quantified and
235 are all reported in Supp. Table 7. For major elements, samples were first melted with lithium
236 metaborate. Metaborate fusion products were then dissolved with nitric acid and like for
237 biological samples, concentrations were determined on an ICP-AES (Agilent 5800). Loss on
238 ignition (LOI) was measured by weighing the bulk sample before and after 1 h of calcination
239 at 1000 °C. For trace elements, samples were directly dissolved in a concentrated HF-HNO₃
240 (1:3) mixture at 90 °C for at least 48 h before evaporation and resuspension in a concentrated
241 HNO₃ - 6N HCl (1:1) mixture at 90 °C for 24 h. This step was repeated three times. Trace
242 element concentrations were measured on a quadrupole ICP-MS (Agilent 7500). Both
243 accuracy and reproducibility of the major and trace element contents were monitored by
244 replication of international rock standards (BHVO₂). The concentration obtained for the
245 standards are in agreement with the reference values, and reproducibility is, on average, better
246 than 5% for the trace and 10% (2sd) for the major elements (see Supp. Table 7).

247 Note that beyond the total digestion procedure used in this study to assess the entire
248 metallomic signature of the geological samples, another parameter termed the bioaccessibility
249 (performed with water, synthetic gastric and/or lung fluids) may help to refine metal exposure
250 assessment³⁷⁻³⁹. In this preliminary study, in the absence of established analytical protocols
251 and the lack of significant databases, in particular with regard to isotopic data, we however
252 undertook to first maximize the risk resulting from metallome deregulations induced by long-
253 term volcanic ash exposure via a total dissolution procedure. In future studies, measuring the
254 chemical and for the first time the copper and zinc isotopic bioaccessibility might however be
255 useful to better constrain this volcanic hazard.

256

257 **2.5. Cu and Zn isotopic compositions**

258 Copper (Cu) and zinc (Zn) isotopic compositions were measured following the procedure
259 described by Maréchal et al.⁴⁰. Cu and Zn were purified using quartz columns filled with 1.8
260 mL of Bio-Rad AG MP-1 (100-200 mesh) anion exchange resin. After removing the matrix
261 phase with 10 mL of 7N HCl + 0.001% H₂O₂, Cu was first eluted with 20 mL of the same
262 solution, followed by Zn with 10 mL of a 0.5N HNO₃ solution. Total procedural blanks were less
263 than 6 ng for Zn and lower than 2 ng for Cu which is well below the amount of these elements
264 in all the samples (on average Zn and Cu > 200 ng except for urine in which Zn and Cu ~ 50
265 ng).

266 Isotopic compositions were measured on a Thermo Scientific Neptune Plus MC-ICP-
267 MS using standard sample and skimmer cones in wet plasma conditions (*i.e.*, no desolvating
268 nebulizer system (DSN) with cycloning introduction chamber and a 50µL/min glass nebulizer).
269 On the day of the analyses, Zn and Cu purified solutions were diluted in a Cu (Cu SRM 976,
270 National Institute of Standards and Technology, Gaithersburg, MD, USA) and Zn-doped
271 solution (Zn JMC 3-0749L, Johnson Matthey Royston, UK) respectively, to match the
272 concentration of the standard mixture ran between the samples (about 250 µg.L⁻¹). The delta

273 values (expressed in ‰) are reported relative to the isotopic solution reference material NIST
274 SRM 976 for Cu and JMC 3-0749L for Zn and are referred as:

$$275 \quad \delta^{65}\text{Cu}_{\text{sample}} = \left[\frac{\left(\frac{{}^{65}\text{Cu}}{{}^{63}\text{Cu}} \right)_{\text{sample}}}{\left(\frac{{}^{65}\text{Cu}}{{}^{63}\text{Cu}} \right)_{\text{SRM976}}} - 1 \right] * 10^3 \quad \text{and} \quad \delta^{66}\text{Zn}_{\text{sample}} = \left[\frac{\left(\frac{{}^{66}\text{Zn}}{{}^{64}\text{Zn}} \right)_{\text{sample}}}{\left(\frac{{}^{66}\text{Zn}}{{}^{64}\text{Zn}} \right)_{\text{JMC3-0749L}}} - 1 \right] * 10^3$$

276 Instrumental mass fractionation was corrected with an exponential law using an elemental-
277 doping method and instrumental drift over time was controlled with standard sample
278 bracketing⁴⁰.

279 The long-term precision of the results was assessed by sample re-run analysis (bis) and
280 repeated measurements of the pure Cu SRM 976 and Zn JMC 3-0749L standard solutions run
281 every two samples and the accuracy was assessed by the measurement of biological (1577c)
282 and geological (BHVO₂) international reference materials. The reproducibility (2sd) of the Cu
283 SRM 976 and Zn JMC 3-0749L standards was better than 0.07‰ (n=150) for both $\delta^{65}\text{Cu}$ and
284 $\delta^{66}\text{Zn}$. Our results for the reference standards are 0.08 ‰ (2sd, n=8) for 1577c and 0.04 ‰
285 (2sd, n=5) for BHVO₂ for $\delta^{65}\text{Cu}$ ($\delta^{65}\text{Cu}_{1577\text{c}} = +0.27 \pm 0.08$ (2sd, n = 8), $\delta^{65}\text{Cu}_{\text{BHVO}_2} = +0.06 \pm$
286 0.04 (2sd, n = 5)) and are 0.04 ‰ (2sd, n=8) for 1577c and 0.01 ‰ (2sd, n=5) for BHVO₂ for
287 $\delta^{66}\text{Zn}$ ($\delta^{66}\text{Zn}_{1577\text{c}} = -0.21 \pm 0.04$ (2sd, n = 8), $\delta^{66}\text{Zn}_{\text{BHVO}_2} = +0.32 \pm 0.01$ (2sd, n = 5) (cf Supp.
288 Tables 2 and 7). All these values are in good agreement with certified and previous published
289 values *i.e.*, $\delta^{65}\text{Cu}_{1577\text{c-ref}} = +0.37 \pm 0.05$ (2sd) and $\delta^{66}\text{Zn}_{1577\text{c-ref}} = -0.19 \pm 0.05$ (2sd)⁴¹ and
290 $\delta^{65}\text{Cu}_{\text{BHVO}_2\text{-ref}} = +0.09 \pm 0.06$ (2sd) and $\delta^{66}\text{Zn}_{\text{BHVO}_2\text{-ref}} = +0.27 \pm 0.05$ (2sd) (source: Georem).
291 Given our long-term precision and the accuracy obtained on reference material
292 measurements, the two-standard deviation (2sd) analytical uncertainty adopted in this study
293 for the Cu and Zn isotopic compositions is ± 0.07 ‰.

294 3. Results

295 3.1. Geological samples

296 The lab-crushed volcanic ash has a median grain size of ~100 μm (3.5 Φ) (Supp. Figure 1b). It
297 has a dacitic composition with a high SiO₂ (69.25 ± 0.60 % (2sd), n = 5) and a low Na₂O+K₂O
298 (1.83 ± 0.22 % (2sd), n = 5) content (Supp. Figure 1c). More generally, it has relatively high
299 major element contents (Ti, Al, Fe, Mn, Mg, Ca, Na and K) compared to a wide spectrum of
300 worldwide volcanic ash, although these values remain lower or equivalent to those measured
301 in the upper continental crust (UCC) (Supp. Figure 3). Inversely, for trace elements and more
302 particularly metals, it has relatively high values compared to previously reported data for
303 several worldwide volcanic ash which can exceed the average UCC values (enrichment factor
304 > 1) as shown for example for vanadium (V), copper (Cu), molybdenum (Mo) and cadmium
305 (Cd) (Supp. Figure 3). Regarding the stable isotopic compositions, La Soufrière volcanic ash
306 has a copper and zinc isotopic composition of -0.52 ± 0.11 ‰ (2sd, n = 5) and $+0.18 \pm 0.02$ ‰
307 (2sd, n = 5) respectively (cf Supp. Table 7).

309 3.2. Trace element concentrations and Cu-Zn isotopic compositions in 310 biological samples

311 To evaluate the effect of chronic exposure to metal-rich volcanic ash on the entire body
312 metallome, we used significant p-value boxplots (Supp. Figure 4) and principal component
313 analyses (PCA) (Figure 2). Briefly, PCA is a mathematical algorithm that reduces the
314 dimensionality of an original multivariate dataset by identifying new variables (principal
315 components; PCs), defined as linear combinations of the original variables⁴². Such multivariate
316 analysis method allows to preserve and visualize the main relevant information in a new PC1
317 vs PC2 space. Our results show that, independently of ash exposure, the mice metallome is
318 organ-specific (Figure 2 and Supp. Figure 5) and isotopically-typified (Figure 3) as previously
319 described in the literature^{43,44}. After one month of ash exposure, the latter tend to be highly
320 disrupted as shown for example by the significant (p-value < 0.05) heavy and alkaline metal
321 accumulation (Zn, Fe, Mn, Ca, Mg, K, P) (Supp. Figure 4) associated to an upward trend for
322 copper (Figure 4a), cobalt and vanadium ($0.05 < \text{p-value} < 0.1$) in the testes. Similarly, after
323 one month of exposure, the blood reservoir is significantly enriched (p-value < 0.05) in

324 vanadium (V), iron (Fe) selenium (Se) and cerium (Ce) (Supp. Figure 4). When still focusing
325 on the elemental concentrations, the intestine, the brain, the lung, the heart and the kidney are
326 also subjected to metallome deregulations but to a lesser extent. For example, the only major
327 variation observed in the lung is limited to V increase while for the intestine the V, Fe and Co
328 enrichments are counterbalanced by strontium (Sr), manganese (Mn), Cu, arsenic (As) and
329 calcium (Ca) decrease (Supp. Figure 4). Another noticeable feature, so far never observed, is
330 the significant ~0.3 ‰ copper isotopic decrease observed in liver and intestine in association
331 to a Cu drop after one month of exposure (Figure 3a and Supp. Figure 4) associated with small
332 but not significant zinc isotopic variations in blood, urine and kidney (Figure 3b).
333 All these results, besides complementing previous studies, show for the first time that, in
334 addition to external body parts like urine, scalp hair¹⁸ or mice tail⁴⁵, internal organs are also
335 significantly affected by metallome disruption. Note that all these elemental deregulations are
336 organ and fluid-dependent, with testes, blood, urine and to a lesser extent liver presenting a
337 more pronounced disrupted metallome as illustrated by significant differences between the
338 control and the exposed subjects (Figure 2a and Supp. Figure 4) than lung, brain, kidney, heart
339 and intestine characterized by a more stable metallome over time exposure (Figure 2b and
340 Supp. Figure 4).

341 3.3. Ash-related pathophysiological deregulations

342 In association with internal metallome deregulations, we observed external and morphological
343 features after one month of exposure. The most obvious is a decrease of food (Supp. Figure
344 2a) and water (Supp. Figure 2b) consumption although this has no direct impact on the body
345 weight (Supp. Figure 2c). From a physiological point of view, our results demonstrate that the
346 organs mostly affected by metallome deregulation (*i.e.*, testes, liver) are also marked by more
347 pronounced physiological disturbances while all the other organs like kidney and lung maintain
348 a stable structure over time exposure with no signs of evident intra-tissue damages
349 (histological data not shown here). For testes, the main changes translate into a minimum 25
350 % decrease of spermatozoa in the head and in the tail of the epididymis *i.e.*, inadequate
351 number of male germ cells (Figure 4b) associated with a significant number of visible
352 microscopic lesions in the male reproductive system as highlighted by lower testicular
353 epithelium thickness ($p_{\text{Mann-Whitney U-test}}=0.002$; Figure 4c), epithelial desquamation (Figure 5b,c),
354 intratubular atypical germ cells (Figure 5d) and preliminary signs of interstitial fibrosis (Figure
355 5c), all accounting for significant tubular degeneration. Our results also demonstrates that
356 volcanic ash exposure led to a significant decrease of the number of spermatids ($p=0.039$)
357 associated to a downward trend to lower Sertoli cells number ($p=0.1797$), as revealed by
358 acetyl-Histone H4 (H4ac.) and SOX9 immunostaining (Figure 6a). Inversely, the number of
359 spermatogonia and spermatocytes seems to be preserved as shown by the similar number
360 ($p>0.2$) of seminiferous tubules marked by positive PLZF and SYCP3-stained cells in the
361 control and the exposed group (Figure 6a). Altogether, these results suggest that chronic
362 volcanic ash exposure seems to preferentially affect the last stages of spermatogenesis *i.e.*,
363 spermatidogenesis and spermiogenesis without altering stem cells and spermatocytogenesis.
364 Note that like for the decrease of the testicular epithelium thickness (Figure 4c), the most
365 significant spermatids loss is observed in the exposed mice characterized by elevated amount
366 of testicular heavy metals like Fe and Cu (Figure 6b and 6c).
367 For liver, although the histological sections do not show distinctive signs between the control
368 and the exposed mice (not shown here), a significant decrease of the hepatic mass ($p_{\text{Mann-Whitney U-test}}=0.002$)
369 was noticed in the exposed mice in association with the copper isotopic
370 decrease (Figure 7a).

372 4. Discussion

373 4.1. Volcanic-ash: a metal-rich reservoir that contributes to organ-specific 374 metallome deregulations

375 In volcanic areas, the consumption of food^{16,46} and water^{15,47} contaminated by volcanogenic
376 elements have been demonstrated to significantly biocontaminate the residents, as
377

378 documented by higher trace element contents in urine¹⁵ and scalp hair¹⁸ of people living in
379 the vicinity of an active volcano compared to people of control areas. Over time, such volcanic-
380 derived metallome disturbances might contribute to significant health risk and favor the
381 development of severe diseases like thyroid cancer^{15,48}, although, to our knowledge, no
382 metallomic data has yet been reported for thyroid glands and more generally for vital organs
383 to support this assumption. As the food chain is an important route of metal human exposure,
384 other and more direct contamination induced for example by long-term exposure and
385 subsequent ingestion of volcanic ash could also contribute to severe metal contamination.
386 As they make up the majority of volcanic soils⁴⁹, volcanic ash can be easily remobilized and
387 absorbed by the organism, either by oral or dermal routes (up to 1000 mg per day⁵⁰ by oral
388 ingestion) or by inhalation. La Soufrière volcanic ash is enriched in several chemical elements
389 and particularly heavy metals such as Cu, Mo, V, Co, Cd, Fe and Mn, with values exceeding
390 the ones reported for the upper continental crust (UCC) and well above the average content
391 reported in several worldwide volcanic ash (Supp. Figure 3). Then, La Soufrière volcanic ash
392 appears as an important metal reservoir to which direct and/or indirect (via food and water
393 transfer) prolonged exposure may significantly deregulate the inner metallome. Our results
394 demonstrate that, independently of ash exposure, the mice metallome is organ-specific (Supp.
395 Figure 5) and isotopically-typified (Figure 3) as previously described^{43,51,52}. However, after one
396 month of exposure to metal-rich volcanic ash, the latter turn out to be highly disrupted,
397 translating into both major and trace elements (Figure 2 and Supp. Figure 4) as well as $\delta^{65}\text{Cu}$
398 and $\delta^{66}\text{Zn}$ changes (Figure 3). Observed for the first time in inner organs, these variations are
399 not systematic but rather organ-specific, with the liver and testes, in tandem with blood and
400 urine (Figure 2a and Supp. Figure 4), being preferentially affected; as illustrated by more
401 pronounced ash exposure-related metallome variations; compared to the brain, lung, heart,
402 kidneys and intestine presenting a relatively more stable (e.g. lung) and/or counterbalanced
403 (e.g. intestine) metallome over time exposure (Figure 2b and Supp. Figure 4). The most
404 important variations are noted in testes (Figure 2a and Supp. Figure 4), the latter being
405 characterized by a significant enrichment ($p_{\text{wilcoxon-test}} < 0.05$) in Zn, Fe, Mn, Ca, K, Mg and P
406 (Supp. Figure 4) and an upward trend for Cu, Co and V (e.g. Figure 4a) coupled with no Cu-
407 Zn isotopic drift (Figure 3). Note that a similar enrichment tendency is also found in the blood
408 reservoir as shown for example by higher V ($p_{\text{wilcoxon-test}}=0.002$) and Fe ($p_{\text{wilcoxon-test}}=0.026$)
409 content in the exposed mice. The testicular heavy metal accumulation may result from the
410 progressive disruption of the hemato-testicular barrier. As shown on Figure 6a, mice exposed
411 to volcanic ash are characterized by a downward trend to lower Sertoli cells number in
412 seminiferous tubules compared to the control mice, as demonstrated by the lower number of
413 seminiferous tubules marked by positive SOX9-stained cells in the exposed group
414 ($\text{SOX9}^+_{\text{cells}}=9.63\pm 3.67$ (1sd)) versus the control group ($\text{SOX9}^+_{\text{cells}}=12.16\pm 2.87$ (1sd)). Sertoli
415 cells are somatic cells that form the blood-testis barrier and any decline, will directly translate
416 into a progressive rupture of this barrier, favoring the transfer of heavy metals from the blood
417 to the testis. The liver is inversely marked by a significant drop in $\delta^{65}\text{Cu}$ (Figure 7) but a less
418 pronounced major and trace content changes limited to the drop of copper (Supp. Figure 4),
419 appearing as a more distinct case. Compared to the testes, the liver is a central organ in metal
420 homeostasis that ensures a set of metabolic functions essential for the organism. By
421 accounting for a large fraction of body metals such as copper, the liver stores, redistributes
422 and excretes metal excess through urine, feces and bile⁵³. The limited hepatic variations
423 denoted for elemental concentrations is thus likely counterbalanced by preferential testicular
424 and to a lesser extent blood metal accumulation and might result from an amplified protective
425 mechanism resulting in higher metal urinary excretion, as supported by elevated chemical
426 contents measured in the urine of exposed mice (see Figure 2a and Supp. Table 2). Altogether,
427 these results suggest that liver functions, despite the presence of copper isotopic disruptions,
428 tend to be maintained after one month of exposure to volcanic ash. Taken as a whole, all these
429 results demonstrate that metal-rich volcanic ash acts as an external perturbation that rapidly
430 disrupts the inner metal homeostasis at the entire body scale.
431

4.2. Ash-related metallome deregulation and early pathophysiological modifications: the case of the testes

Metals like copper (Cu), zinc (Zn) and iron (Fe) are involved in several enzymes and proteins that regulate a set of metabolic pathways essential for the body functions including but not limited to cell energy (ATP) production, reactive oxygen species (ROS) detoxification^{53,54}, spermatogenesis⁵⁵ and immune functions⁵⁶. Metals are thus vital in the organism, but any homeostatic disturbance (accumulation, deficit, mislocalization as well as isotopic variation), as induced by chronic volcanic ash exposure (*cf* section 4.1), can play a reverse role in these processes and subsequently represent a significant health risk. Cu metallome deregulation is for example associated to neurodegenerative diseases^{23,57} and cancer⁵⁸ development. Despite the well-established toxic effect of some metals and the recent observation that mammals (human and animal) living in a volcanic area are more prone to develop testicular damages⁴⁵, multiple sclerosis¹⁴ and cancers^{15,16}, whether volcanic ash-derived metallome deregulation contributes to pathological dysfunctions and incidence of diseases in the volcanic areas has to be better constrained.

As detailed above, testes are the first organs severely affected by volcanic ash-induced metallome deregulation (Figure 2a and Supp. Figure 4). This preferential and targeted metallic disruption is associated with significant tubular degeneration as highlighted by inadequate number of germ cells including spermatids (Figure 6a) and spermatozoa in the head and the tail of the epididymis (Figure 4b). After one month of metal-rich volcanic ash exposure, significant microscopic lesions are also observed in the male reproductive system as shown by lower epithelium thickness (Figure 4c) associated with preliminary signs of epithelial desquamation (Figure 5b, c), interstitial destructuration and inflammation (fibrosis) (Figure 5c). Testes of mice exposed to volcanic ash present also a larger number of uncommitted and atypically-localized intratubular germ cells within the seminiferous tubules strongly resembling to the so-called atypical residual bodies (Figure 5d); as many symptoms, although present in small quantity, that remain absent in the control group (Figure 5a). Abnormal residual bodies (ARB) have been described as the result from impaired maturation of germ cells and/or altered Sertoli cell processing of these remnants, reflecting germ cell degeneration⁵⁹. Although their origin is still unclear, they have been described in rats following administration of tri-*o*-cresyl phosphate⁶⁰ and of a by-product of water disinfection, dibromoacetic acid⁶¹ appearing as a chemically treatment-related fingerprint. In this study, the higher incidence of ARB-like compounds coupled with lower spermatozoa and spermatids as well as a decreased epithelium thickness observed on mice presenting the most pronounced testicular metallome deregulation (Figures 4b, 4c and Figures 6b, 6c) may thus attest of a metal-rich ash exposure-mediated testicular toxicity preferentially resulting from altered spermatido- and spermiogenesis. This observation is further supported by previous studies demonstrating that excess of Cu and other heavy metals such as Pb and Cd, reduce sperm count, mobility, vitality and morphology and subsequently affect male reproductive capacity^{62,63}. In excess, heavy metals can also favor the production of reactive oxygen species (ROS) via the Fenton reaction⁶⁴ that may also contribute to testicular defects and subsequent infertility⁶⁵. Altogether, these results show that volcanic ash-derived metallome deregulations is far from trivial and may, to a certain extent, contribute during lifetime to severe fertility disorders.

4.3. Copper and zinc isotopic compositions: a promising tool to diagnose hepatic ash-related dysfunctions?

Beyond elemental concentrations, another significant metallomic parameter disrupted by volcanic ash exposure and observed for the first time in this study is Cu isotopic decrease in both liver and intestine (Figure 3) and, in a less pronounced way, Zn isotopic fractionation in blood, urine and kidney respectively. Independent of the amount of metals, the Cu and Zn isotopic compositions ($\delta^{65}\text{Cu}$, $\delta^{66}\text{Zn}$) are promising tools that recently offer a more comprehensive view of several biological processes than concentrations alone such as aging^{20,21,66}. They also turned out to be very promising tools for pointing out a disruption in the oxidative stress status⁶⁷, a major pathogenetic event occurring in several liver disorders⁶⁸, and more broadly for the diagnosis, prognosis and follow-up of patients suffering from severe

487 pathologies like cancers^{22,69}, neurodegenerative diseases^{23,70,71} as well as severe hepatic
488 syndromes⁷²⁻⁷⁵; with the amplitude of the variations being likely linked to the severity of the
489 disease^{73,75}. Despite this proven interest, the use of $\delta^{65}\text{Cu}$ and $\delta^{66}\text{Zn}$ as a potential marker for
490 health prevention have never been investigated in a volcanically active context. Here we
491 demonstrate that mice exposed to volcanic ash present a significant hepatic $\delta^{65}\text{Cu}$ drop,
492 following a pattern similar to mice suffering from hepatic diseases⁷² and associated with a
493 hepatic mass loss up to 20% (Figure 7a). Organ weight, and more specifically liver mass loss,
494 is an important parameter for the evaluation of toxicity. Described as a common background
495 finding in elderly⁷⁶ and attributed to portal venous blood flow (PVBF) disturbance⁷⁷, PVBF-
496 related liver mass reduction is also an ubiquitous pattern observed in patients suffering from
497 severe liver diseases such as hepatocellular carcinoma (HCC) and liver cirrhosis⁷⁸. Hepatic
498 mass loss was also noticed in rats' livers in response to increase oxidative stress caused by
499 metal exposure⁷⁹. In the absence of age variations and other markers commonly associated
500 with advanced liver dysfunctions such as histological lesions, the hepatic mass loss in
501 correlation with the $\delta^{65}\text{Cu}$ decrease (Figure 7a) might be considered as the preliminary warning
502 signs of an ongoing severe liver metabolic disruption. At this stage, the cause of these copper
503 isotopic fractionations remains to be elucidated, but given previous studies, the latter may
504 result from modified copper protein expression, including the superoxide dismutase (Cu-Zn
505 SOD1) in association to enhanced oxidative conditions. These two parameters, identified as
506 precursors in the development of hepatocellular carcinoma⁸⁰, have been demonstrated to
507 impact copper isotopic fractionation^{67,81}.

508 More broadly, hepatic $\delta^{65}\text{Cu}$ decrease may also reflect ongoing impairments that could be
509 generalized at the entire enterohepatic cycle. As shown on Figure 3a and Supp. Figure 6, after
510 one month of exposure, the hepatic $\delta^{65}\text{Cu}$ decrease is associated with a significant intestinal
511 $\delta^{65}\text{Cu}$ drop. Although the most evident process to explain such Cu isotopic variability is the
512 presence of volcanic particles having light Cu isotopic composition ($\delta^{65}\text{Cu}_{\text{ash}}=-0.52\pm 0.11\%$) in
513 the liver and the intestinal tractus, none were observed in any of the histologically quantified
514 organs including liver. Inversely, intestinal Cu uptake is largely mediated by two major
515 membrane transporters (CTR1 and DMT1) and metalloredutase (STEAP proteins)⁵³ which
516 alteration has been demonstrated to significantly affect $\delta^{65}\text{Cu}$ ⁸². The light intestinal $\delta^{65}\text{Cu}$
517 observed in the exposed mice thus likely results from impaired Cu gut uptake, directly echoing
518 to altered food consumption (Supp. Figure 2). Once absorbed, Cu is incorporated into the
519 nutrient rich blood and transported through the portal vein from the gut to the liver. This
520 subsequently impacts the $\delta^{65}\text{Cu}$ liver as supported by the correlation observed between
521 hepatic and intestinal $\delta^{65}\text{Cu}$ (Supp. Figure 6).

522 Monitoring liver $\delta^{65}\text{Cu}$ may thus offer new perspectives to alert on the early development of
523 (entero)hepatic deregulations in volcanic areas. The measurement of hepatic $\delta^{65}\text{Cu}$ will
524 however require a biopsy *i.e.* an invasive surgical intervention that may limit the scope of this
525 marker. But this might be overcome with less invasive blood tests. As highlighted on Figure
526 7b, the hepatic $\delta^{65}\text{Cu}$ correlates with the blood $\delta^{66}\text{Zn}$, suggesting that the blood $\delta^{66}\text{Zn}$ might be
527 an equally robust but far less invasive biomarker. To date, although the simultaneous
528 measurement of hepatic $\delta^{65}\text{Cu}$ and blood $\delta^{66}\text{Zn}$ remains mandatory to ensure that the blood
529 isotopic variations really reflect hepatic disorders, in the future, this will allow to move towards
530 less invasive techniques only focused on blood isotopic analyses. All these results, beyond
531 being innovative, are highly promising for all countries with a large population living in proximity
532 to the volcanoes such as Peru, marked by an atypical age-specific pattern of hepatocellular
533 carcinomas (HCCs)⁸³, and more generally for developing countries in which more than 80% of
534 HCCs occur⁸⁴ and for which, no reliable diagnosis markers are currently available⁸⁵.

535

536 5. Conclusions and Perspectives

537 Our study reveals that mice chronically exposed to volcanic ash deposits present an organ-
538 specific and isotopically-typified metallome deregulation. These deregulations, observed for
539 the first time at the whole-body scale, confirm that volcanic ash is a major metal-rich
540 contaminant that can seriously influence exposure to and intake of trace elements. In addition

541 to urine and blood, testes and, to a lesser degree, liver turned out to be preferentially affected
542 by these ash-related metallome disruptions, which, after a month, are associated with
543 pronounced pathophysiological changes. In the testes, this translates into an alteration of the
544 spermatogenesis, attesting of a metal-rich ash exposure-mediated testicular toxicity. Beyond
545 chemical concentrations, copper and zinc stable isotopic compositions were, for the first time,
546 quantified at the entire body scale. Our results demonstrate that the liver, the intestine and to
547 a lesser extent the blood are affected by $\delta^{65}\text{Cu}$ and $\delta^{66}\text{Zn}$ variations, that may be interpreted
548 as the warning signs of coming up (entero)hepatic diseases. The analysis of hepatic $\delta^{65}\text{Cu}$ and
549 blood $\delta^{66}\text{Zn}$, may thus appear as a promising and innovative technique to diagnose severe
550 liver dysfunctions preponderant in some developing and volcanic countries. In perspective,
551 bio- and isotopically-monitoring human fertility and more broadly (entero)hepatic disorders in
552 populations living in volcanic areas would bring valuable insights to confirm the findings of this
553 study.

554

555 **Acknowledgements**

556 We gratefully acknowledge Jean-Marie Nedelec of the Chemistry Institute of Clermont-Ferrand
557 (ICCF) for his help in the grainsize characterization of the geological ash samples as well as
558 Chantal Bosq, Abdel-Mouhcine Gannoun, Jean-Luc Piro, Mhammed Benbakkar and Claire
559 Fonquernie of the Laboratoire Magmas and Volcans (LMV) for their assistance in the clean
560 laboratory as well as during isotopic, trace and major element measurements respectively. We
561 are also grateful to Fanny Perrière (Laboratoire Microorganismes, Génome Environnement,
562 LMGE) for her technical support to freeze-dry the biological samples. Thanks are also due to
563 Sandrine Plantade, Khirredine Ouchen, Philippe Mazuel for their help at the animal facility as
564 well as Laura Thirouard and Sabrina Dehay of the Institute of Genetics, Reproduction and
565 Development (iGReD) for helping us in the histological data preparation and interpretation. We
566 also thank the AniPath platform from the iGReD for histological analyses. This research was
567 financed by the French government IDEX-ISITE initiative 16-IDEX-0001 (CAP 20-25). This is
568 a Laboratory of Excellence ClerVolc contribution number 513.

569

570 **References**

- 571 1. Takahashi, T. & Shoji, S. Distribution and Classification of Volcanic Ash Soils.
572 *Global Environ. Res.* **6**, 16 (2001).
- 573 2. Small, C. & Naumann, T. The global distribution of human population and recent
574 volcanism. *Environmental Hazards* **3**, 93–109 (2001).
- 575 3. Shoji, S., Dahlgren, R. & Nanzyo, M. Chapter 1 Terminology, Concepts and
576 Geographic Distribution of Volcanic Ash Soils. in *Developments in Soil Science* vol. 21 1–5
577 (Elsevier, 1993).
- 578 4. Simkin, T. & Siebert, L. *Earth's volcanoes and eruptions: an overview*. Sigurdsson,
579 H. (ed.), *Encyclopedia of Volcanoes*. San Diego: Academic, pp. 249–262. (2000).
- 580 5. Ayris, P. M. & Delmelle, P. The immediate environmental effects of tephra emission.
581 *Bull Volcanol* **74**, 1905–1936 (2012).
- 582 6. Tomašek, I. *et al.* Assessing the biological reactivity of organic compounds on
583 volcanic ash: implications for human health hazard. *Bull Volcanol* **83**, 30 (2021).
- 584 7. Green, F. H. Y. *et al.* Is volcanic ash a pneumoconiosis risk? *Nature* **293**, 216–217
585 (1981).
- 586 8. Lee, S. H. & Richards, R. J. Montserrat volcanic ash induces lymph node granuloma
587 and delayed lung inflammation. *Toxicology* **195**, 155–165 (2004).
- 588 9. Sanders, C. L., Rhoads, K. & Mahaffey, J. A. Long-Term Reactivity of Lung and
589 Mediastinal Lymph Nodes following Intratracheal Instillation of Sandy Loam Soil or Mount
590 St. Helens Volcanic Ash'. *Environmental Research* **32**, 188–198 (1983).
- 591 10. Aguilera, C. *et al.* Biological Impact of Exposure to Extremely Fine-Grained Volcanic
592 Ash. *Journal of Nanotechnology* **2018**, 1–12 (2018).
- 593 11. Damby, D. E. *et al.* Volcanic Ash Activates the NLRP3 Inflammasome in Murine and

- 594 Human Macrophages. *Front. Immunol.* **8**, 2000 (2018).
- 595 12. Damby, D. E., Murphy, F. A., Horwell, C. J., Raftis, J. & Donaldson, K. The in vitro
596 respiratory toxicity of cristobalite-bearing volcanic ash. *Environmental Research* **145**, 74–84
597 (2016).
- 598 13. Baxter, P. J., Ing, R., Falk, H. & Plikaytis, B. Mount St. Helens Eruptions: The Acute
599 Respiratory Effects of Volcanic Ash in a North American Community. *Archives of*
600 *Environmental Health: An International Journal* **38**, 138–143 (1983).
- 601 14. Nicoletti, A. *et al.* Incidence of multiple sclerosis in the province of Catania. A geo-
602 epidemiological study. *Environmental Research* **182**, 109022 (2020).
- 603 15. Malandrino, P. *et al.* Increased thyroid cancer incidence in a basaltic volcanic area is
604 associated with non-anthropogenic pollution and biocontamination. *Endocrine* **53**, 471–479
605 (2016).
- 606 16. Türkdoğan, M. K., Kilicel, F., Kara, K., Tuncer, I. & Uygan, I. Heavy metals in soil,
607 vegetables and fruits in the endemic upper gastrointestinal cancer region of Turkey.
608 *Environmental Toxicology and Pharmacology* **13**, 175–179 (2003).
- 609 17. Leung, C. C., Yu, I. T. S. & Chen, W. Silicosis. *The Lancet* **379**, 2008–2018 (2012).
- 610 18. Varrica, D., Tamburo, E., Dongarrà, G. & Sposito, F. Trace elements in scalp hair of
611 children chronically exposed to volcanic activity (Mt. Etna, Italy). *Science of The Total*
612 *Environment* **470**, 117–126 (2014).
- 613 19. Lobinski, R., Becker, J. S., Haraguchi, H. & Sarkar, B. Metallomics: Guidelines for
614 terminology and critical evaluation of analytical chemistry approaches (IUPAC Technical
615 Report). *Pure and Applied Chemistry* **82**, 493–504 (2010).
- 616 20. Sauzéat, L., Laurençon, A. & Balter, V. Metallome evolution in ageing *C. elegans* and
617 a copper stable isotope perspective. *Metallomics* **10**, 496–503 (2018).
- 618 21. Morel, J.-D. *et al.* The mouse metallomic landscape of aging and metabolism. *Nature*
619 *Communications* **10** (2022) doi:<https://doi.org/10.1038/s41467-022-28060-x>.
- 620 22. Balter, V. *et al.* Natural variations of copper and sulfur stable isotopes in blood of
621 hepatocellular carcinoma patients. *PNAS* **112**, 982–985 (2015).
- 622 23. Sauzéat, L. *et al.* Isotopic Evidence for Disrupted Copper Metabolism in Amyotrophic
623 Lateral Sclerosis. *iScience* **6**, 264–271 (2018).
- 624 24. Guern, F. L., Bernard, A. & Chevrier, R. M. Soufrière of Guadeloupe 1976-1977
625 Eruption - Mass and Energy Transfer and Volcanic Health Hazards (*). *Bulletin of*
626 *Volcanology* **43–3**, 577–593 (1980).
- 627 25. Moretti, R. *et al.* The 2018 unrest phase at La Soufrière of Guadeloupe (French West
628 Indies) andesitic volcano: Scrutiny of a failed but prodromal phreatic eruption. *Journal of*
629 *Volcanology and Geothermal Research* **393**, 106769 (2020).
- 630 26. Jessop, D. E. *et al.* A multi-decadal view of the heat and mass budget of a volcano in
631 unrest: La Soufrière de Guadeloupe (French West Indies). *Bull Volcanol* **83**, 16 (2021).
- 632 27. Bilan mensuel de l'activité volcanique de la Soufrière de Guadeloupe et de la sismicité
633 régionale. OVSG-IPGP Octobre 2021; ISSN 1622-4523. DOI:
634 http://volcano.ipgp.fr/guadeloupe/Bulletins/2021/OVSG_2021-10_fra.pdf. (2021).
- 635 28. Sigurdsson, H., Houghton, B., McNutt, S., Rymer, H. & Stix, J. *The encyclopedia of*
636 *Volcanoes*. (Elsevier Science (Eds.), 2015).
- 637 29. Komorowski, J.-C. *et al.* *Volcanic Hazard Atlas of the Lesser Antilles. Guadeloupe,*
638 *in: Lindsay, J.M., Robertson, R.E.A., Shepherd, J.B., Ali, S. (Eds.), pp. 65-102. (2005).*
- 639 30. Martel, C., Pichavant, M., Balcone-Boissard, H. & Boudon, G. Syn-Eruptive
640 Conditions of the AD 1530 Sub-Plinian Eruption of La Soufrière of Guadeloupe (Lesser
641 Antilles). *Front. Earth Sci.* **9**, 686342 (2021).
- 642 31. Osman, S., Beckett, F., Rust, A. & Snee, E. Sensitivity of Volcanic Ash Dispersion
643 Modelling to Input Grain Size Distribution Based on Hydromagmatic and Magmatic

- 644 Deposits. *Atmosphere* **11**, 567 (2020).
- 645 32. Waterston, R.H., Lindblad-Toh, K. & Birney, E. Initial sequencing and comparative
646 analysis of the mouse genome. *Nature* **420**, 520–562 (2002).
- 647 33. Rosenthal, N. & Brown, S. The mouse ascending: perspectives for human-disease
648 models. *Nat Cell Biol* **9**, 993–999 (2007).
- 649 34. Garçon, M. *et al.* Nitrile, Latex, Neoprene and Vinyl Gloves: A Primary Source of
650 Contamination for Trace Element and Zn Isotopic Analyses in Geological and Biological
651 Samples. *Geostandards and Geoanalytical Research* **41**, 367–380 (2017).
- 652 35. Keyzer, J. J. *et al.* Zinc in plasma and serum: influence of contamination due to the
653 collection tubes. *Pharmaceutisch Weekblad Scientific Edition* **5**, 248–251 (1983).
- 654 36. Williams, D. M. Trace metal determinations in blood obtained in evacuated collection
655 tubes. *Clinica Chimica Acta* **99**, 23–29 (1979).
- 656 37. Goix, S. *et al.* Metal concentration and bioaccessibility in different particle sizes of
657 dust and aerosols to refine metal exposure assessment. *Journal of Hazardous Materials* **317**,
658 552–562 (2016).
- 659 38. Tomašek, I. *et al.* Development of a simulated lung fluid leaching method to assess the
660 release of potentially toxic elements from volcanic ash. *Chemosphere* **278**, 130303 (2021).
- 661 39. Tomašek, I., Mileusnić, M. & Leboš Pavunc, A. Health impact assessment by
662 ingestion of polluted soil/sediment. *MGPB* **31**, 29–39 (2016).
- 663 40. Maréchal, C. N., Télouk, P. & Albarède, F. Precise analysis of copper and zinc
664 isotopic compositions by plasma-source mass spectrometry. *Chemical Geology* **156**, 251–273
665 (1999).
- 666 41. Sauzéat, L. *et al.* Inter-comparison of stable iron, copper and zinc isotopic
667 compositions in six reference materials of biological origin. *Talanta* **221**, 121576 (2021).
- 668 42. Ringnér, M. What is principal component analysis? *Nat Biotechnol* **26**, 303–304
669 (2008).
- 670 43. Balter, V. *et al.* Contrasting Cu, Fe, and Zn isotopic patterns in organs and body fluids
671 of mice and sheep, with emphasis on cellular fractionation. *Metallomics* **5**, 1470 (2013).
- 672 44. Moynier, F., Fujii, T., Shaw, A. S. & Le Borgne, M. Heterogeneous distribution of
673 natural zinc isotopes in mice. *Metallomics* **5**, 693 (2013).
- 674 45. Ferreira, A. F., Garcia, P. V., Camarinho, R. & Rodrigues, A. dos S. Volcanogenic
675 pollution and testicular damage in wild mice. *Chemosphere* **132**, 135–141 (2015).
- 676 46. Orellana, E. *et al.* Heavy Metals in Native Potato and Health Risk Assessment in
677 Highland Andean Zones of Junín, Peru. *JEP* **11**, 921–937 (2020).
- 678 47. Loma, J. D. Arsenic Exposure and Cancer-Related Proteins in Urine of Indigenous
679 Bolivian Women. *Frontiers in Public Health* **8**, 11 (2020).
- 680 48. Vigneri, R., Malandrino, P., Gianì, F., Russo, M. & Vigneri, P. Heavy metals in the
681 volcanic environment and thyroid cancer. *Molecular and Cellular Endocrinology* **457**, 73–80
682 (2017).
- 683 49. Delmelle, P., Opfergelt, S., Cornelis, J.-T. & Ping, C.-L. The Encyclopedia of
684 Volcanoes (Second Edition). *Part IX: Economic Benefits and Cultural Aspects of Volcanism*
685 1253–1264 (2015) doi:10.1016/b978-0-12-385938-9.00072-9.
- 686 50. Moya, J. & Phillips, L. A review of soil and dust ingestion studies for children.
687 *Journal of Exposure Science & Environmental Epidemiology* **24**, 545–554 (2014).
- 688 51. Ma, S. *et al.* Organization of the Mammalian Ionome According to Organ Origin,
689 Lineage Specialization, and Longevity. *Cell Reports* **13**, 1319–1326 (2015).
- 690 52. Zhang, B., Podolskiy, D. I., Mariotti, M., Seravalli, J. & Gladyshev, V. N. Systematic
691 age-, organ-, and diet-associated ionome remodeling and the development of ionomic
692 aging clocks. *Aging Cell* **19**, (2020).
- 693 53. Kim, B.-E., Nevitt, T. & Thiele, D. J. Mechanisms for copper acquisition, distribution

- 694 and regulation. *Nature Chemical Biology* **4**, 176–185 (2008).
- 695 54. Turski, M. L. & Thiele, D. J. New Roles for Copper Metabolism in Cell Proliferation,
696 Signaling, and Disease*. *Journal of Biological Chemistry* **284**, 717–721 (2009).
- 697 55. Vallee, B. L. & Falchuk, K. H. The biochemical basis of zinc physiology.
698 *Physiological Reviews* **73**, 79–118 (1993).
- 699 56. Bonaventura, P., Benedetti, G., Albarède, F. & Miossec, P. Zinc and its role in
700 immunity and inflammation. *Autoimmunity Reviews* **14**, 277–285 (2015).
- 701 57. Barnham, K. J. & Bush, A. I. Metals in Alzheimer’s and Parkinson’s Diseases.
702 *Current Opinion in Chemical Biology* **12**, 222–228 (2008).
- 703 58. Brady, D. C. *et al.* Copper is required for oncogenic BRAF signalling and
704 tumorigenesis. *Nature* **509**, 492–496 (2014).
- 705 59. Creasy, D. *et al.* Proliferative and Nonproliferative Lesions of the Rat and Mouse
706 Male Reproductive System. *Toxicol Pathol* **40**, 40S–121S (2012).
- 707 60. Somkuti, S. Light and electron microscopic evidence of tri-*o*-cresyl phosphate
708 (TOCP)-mediated testicular toxicity in Fischer 344 rats. *Toxicology and Applied*
709 *Pharmacology* **107**, 35–46 (1991).
- 710 61. Linder, R. E. *et al.* Histopathologic changes in the testes of rats exposed to
711 dibromoacetic acid. *Reproductive Toxicology* **11**, 47–56 (1997).
- 712 62. Eidi, M. Seminal plasma levels of copper and its relationship with seminal parameters.
713 *Iranian Journal of Reproductive Medicine* **8**, 60–65 (2010).
- 714 63. Roblero, L., Guadarrama, A., Lopez, T. & Zegers-Hochschild, F. Effect of copper ion
715 on the motility, viability, acrosome reaction and fertilizing capacity of human spermatozoa in
716 vitro. *Reprod. Fertil. Dev.* **8**, 871 (1996).
- 717 64. Betteridge, D. J. What Is Oxidative Stress? *Metabolism* **49**, Issue 2, Supplement 1, 3–
718 8 (2000).
- 719 65. Asadi, N. The Impact of Oxidative Stress on Testicular Function and the Role of
720 Antioxidants in Improving it: A Review. *JCDR* (2017) doi:10.7860/JCDR/2017/23927.9886.
- 721 66. Jaouen, K. *et al.* Is aging recorded in blood Cu and Zn isotope compositions?
722 *Metallomics* **5**, 1016–1024 (2013).
- 723 67. Flórez, M. R., Costas-Rodríguez, M., Grootaert, C., Van Camp, J. & Vanhaecke, F. Cu
724 isotope fractionation response to oxidative stress in a hepatic cell line studied using multi-
725 collector ICP-mass spectrometry. *Anal Bioanal Chem* **410**, 2385–2394 (2018).
- 726 68. Ismail, N. *et al.* Antioxidant enzyme activities in hepatic tissue from children with
727 chronic cholestatic liver disease. *Saudi J Gastroenterol* **16**, 90 (2010).
- 728 69. Larner, F. *et al.* Zinc isotopic compositions of breast cancer tissue. *Metallomics* **7**,
729 112–117 (2015).
- 730 70. Büchl, A., Hawkesworth, C. J., Ragnarsdottir, K. V. & Brown, D. R. Re-partitioning
731 of Cu and Zn isotopes by modified protein expression. *Geochem Trans* **9**, 11 (2008).
- 732 71. Moynier, F., Foriel, J., Shaw, A. S. & Le Borgne, M. Distribution of Zn isotopes
733 during Alzheimer’s disease. *Geochem. Persp. Let.* 142–150 (2017)
734 doi:10.7185/geochemlet.1717.
- 735 72. Costas-Rodríguez, M. *et al.* Body distribution of stable copper isotopes during the
736 progression of cholestatic liver disease induced by common bile duct ligation in mice.
737 *Metallomics* **11**, 1093–1103 (2019).
- 738 73. Costas-Rodríguez, M. *et al.* Isotopic analysis of Cu in blood serum by multi-collector
739 ICP-mass spectrometry: a new approach for the diagnosis and prognosis of liver cirrhosis?
740 *Metallomics* **7**, 491–498 (2015).
- 741 74. Lamboux, A. *et al.* The blood copper isotopic composition is a prognostic indicator of
742 the hepatic injury in Wilson disease. *Metallomics* **12**, 1781–1790 (2020).
- 743 75. Lauwens, S., Costas-Rodríguez, M., Van Vlierberghe, H. & Vanhaecke, F. Cu isotopic

744 signature in blood serum of liver transplant patients: a follow-up study. *Sci Rep* **6**, 30683
745 (2016).

746 76. Kim, I. H., Kisseleva, T. & Brenner, D. A. Aging and liver disease: *Current Opinion*
747 *in Gastroenterology* **31**, 184–191 (2015).

748 77. Zoli, M. Total and functional hepatic blood flow decrease in parallel with ageing. *Age*
749 *and Ageing* **28**, 29–33 (1999).

750 78. Saftoiu, A., Ciurea, T. & Gorunescu, F. Hepatic arterial blood flow in large
751 hepatocellular carcinoma with or without portal vein thrombosis: assessment by
752 transcutaneous duplex Doppler sonography. *European Journal of Gastroenterology &*
753 *Hepatology* **14**, 167–176 (2002).

754 79. Ogunrinola, O. O. *et al.* Effect of Low Level Cadmium Exposure on Superoxide
755 Dismutase Activity in Rat. *Trop. J. Pharm Res* **15**, 115 (2016).

756 80. Wang, Z., Li, Z., Ye, Y., Xie, L. & Li, W. Oxidative Stress and Liver Cancer: Etiology
757 and Therapeutic Targets. *Oxidative Medicine and Cellular Longevity* **2016**, 1–10 (2016).

758 81. Albarède, F. Metal Stable Isotopes in the Human Body: A Tribute of Geochemistry to
759 Medicine. *ELEMENTS* **11**, 265–269 (2015).

760 82. Cadiou, J.-L. *et al.* Copper transporters are responsible for copper isotopic
761 fractionation in eukaryotic cells. *Sci Rep* **7**, 44533 (2017).

762 83. Bertani, S. *et al.* An Atypical Age-Specific Pattern of Hepatocellular Carcinoma in
763 Peru: A Threat for Andean Populations. *PLoS ONE* **8**, e67756 (2013).

764 84. Yang, J. D. & Roberts, L. R. Hepatocellular carcinoma: a global view. *Nat Rev*
765 *Gastroenterol Hepatol* **7**, 448–458 (2010).

766 85. Asrani, S. K., Devarbhavi, H., Eaton, J. & Kamath, P. S. Burden of liver diseases in
767 the world. *Journal of Hepatology* **70**, 151–171 (2019).

768
769
770
771
772
773
774
775
776
777
778
779
780
781
782
783
784
785
786
787
788
789
790
791
792
793
794
795
796
797
798
799

800
801
802
803

Figures:

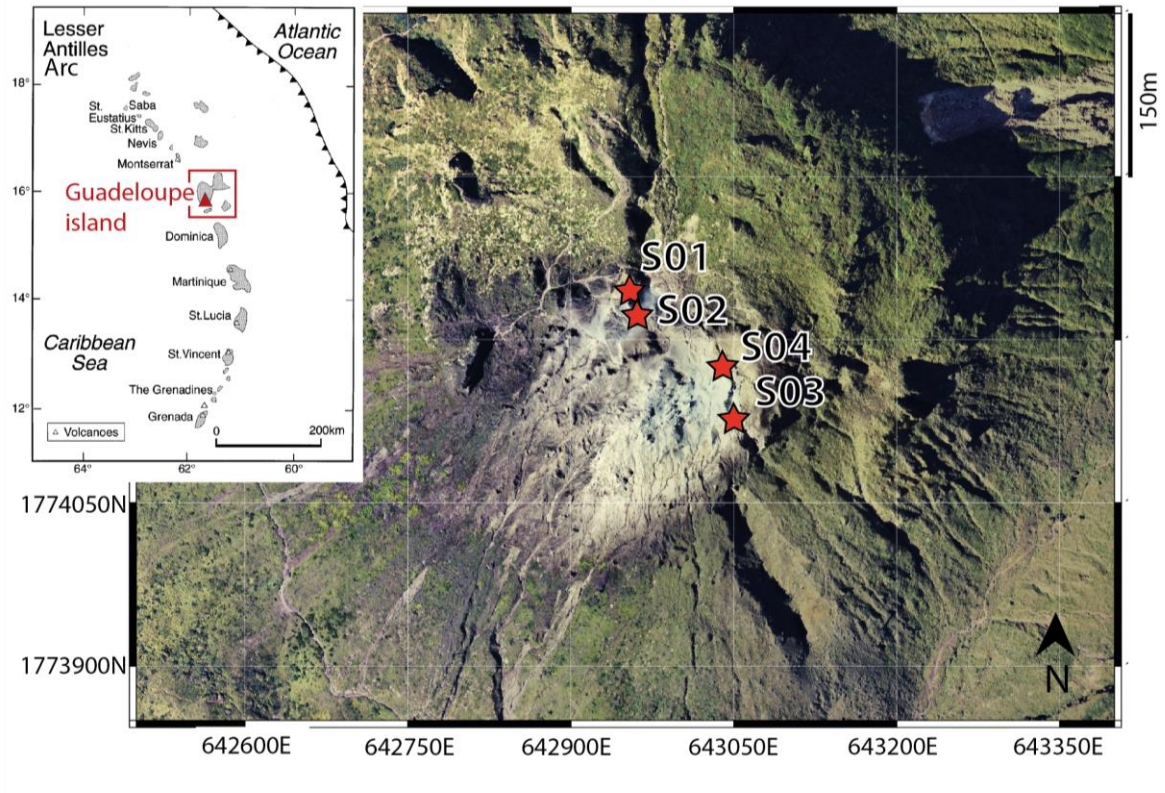


Figure 1: Location map of the studied area

Map of the Soufrière volcano located in the Guadeloupe island (Basse-Terre) of the Lesser Antilles arc (UTM coordinates). The red triangle indicate the location of the Soufrière volcano and the red stars indicate the sampling locations of the rocks from the volcanic dome (S01 to S04) used to reproduce «artificial» volcanic ash later exposed to mice in this study. S01 and S02 were collected on the «Tarissan» site while S03 and S04 are from the «Cratère Sud» site.

804

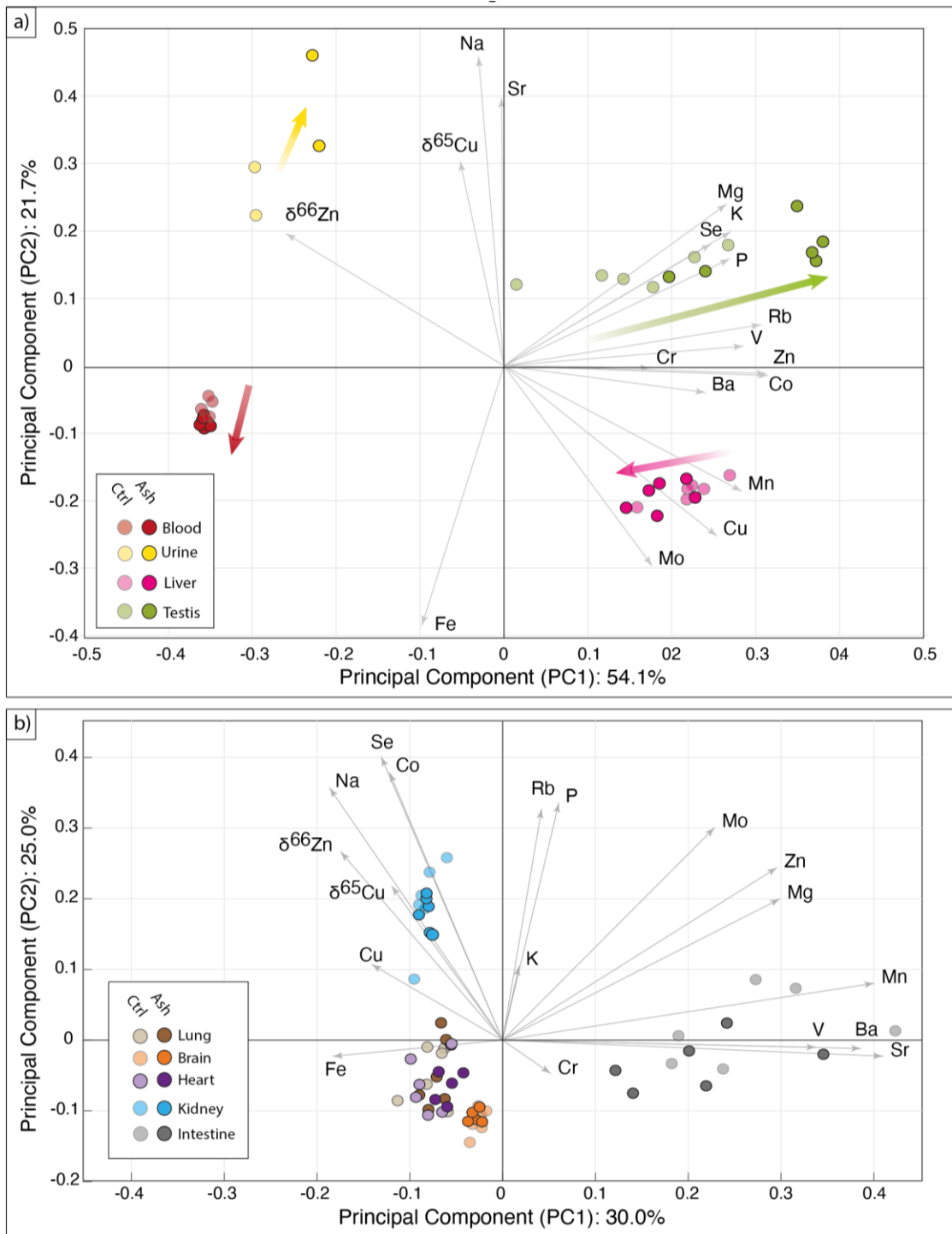


Figure 2. Principal Component Analysis (PCA) of the Results

The PCA allows (a) the identification of organs (i.e. testis and liver) and body fluids (i.e. blood and urine) preferentially affected by metallome deregulation (i.e. metallome difference between control and exposed subjects) due to volcanic ash exposure from (b) those that are less (i.e. no metallome difference between control and exposed subjects). In this study, the variables include the chemical concentrations of 16 major and trace elements measured in 7 organs and 2 biological fluids of mice, as well as $\delta^{65}\text{Cu}$ and $\delta^{66}\text{Zn}$ values. Grey arrows are graphic representations of loading factors in the new PC1 vs. PC2 space. The coordinates of each sample in the new PC1 vs. PC2 space (i.e. sample scores) are shown by circles. Transparency and solid points stand for control and exposed subjects, respectively. All data were normalized, and samples with incomplete data were excluded. PCA was implemented in MATLAB™.

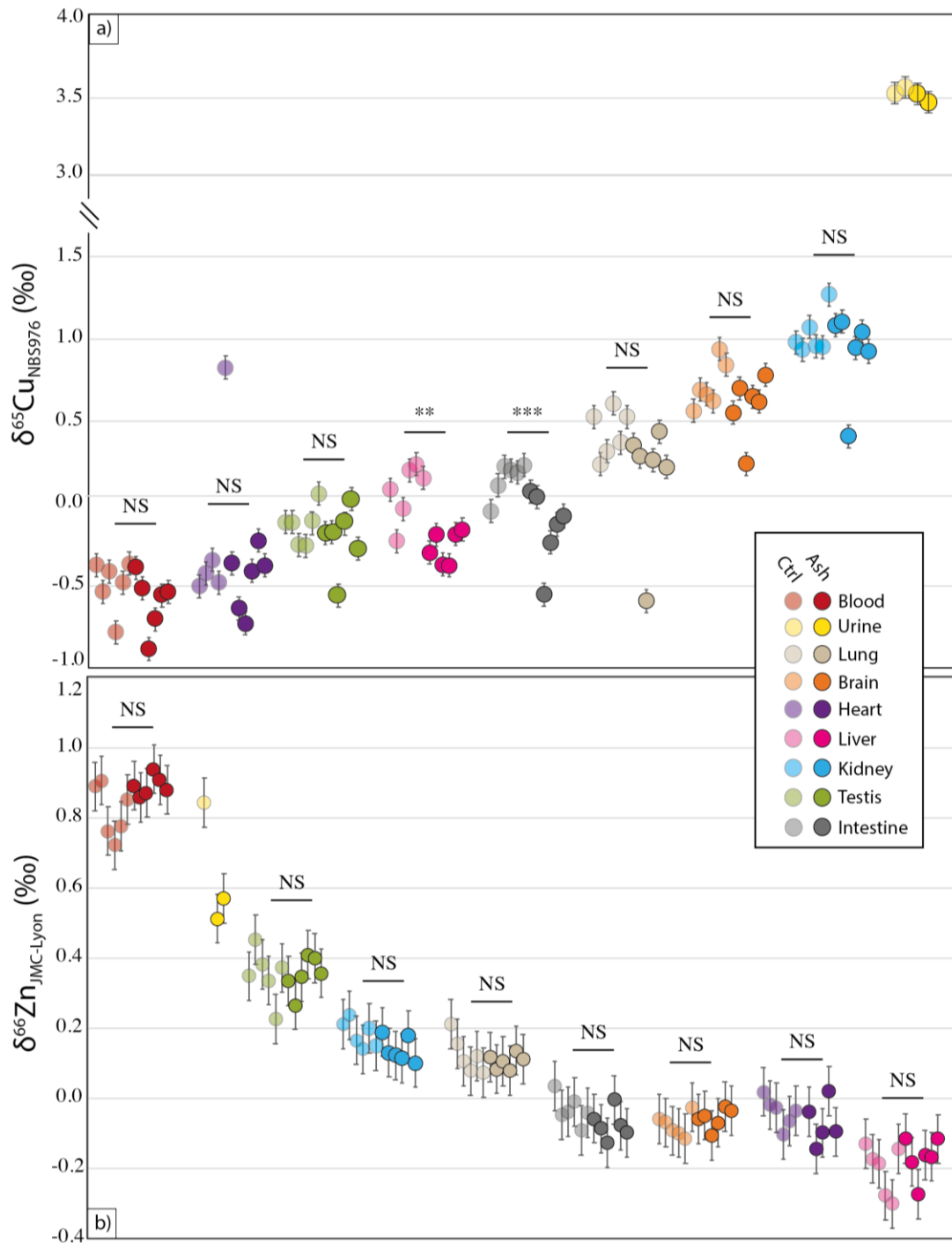


Figure 3: Copper ($\delta^{65}\text{Cu}$) and zinc ($\delta^{66}\text{Zn}$) isotopic compositions of mice body reservoirs

Transparency and solid points stand for control and exposed subjects, respectively. For each reservoirs, the approximate p -value was determined between the control and the exposed group ($n=6$ per group and per reservoir) by a two-sided non-parametric Mann-Whitney U-test implemented in MATLABTM. ** and *** stand for p -value lower than 0.02 and 0.01 respectively. For each datapoint, error bars represent 2sd.

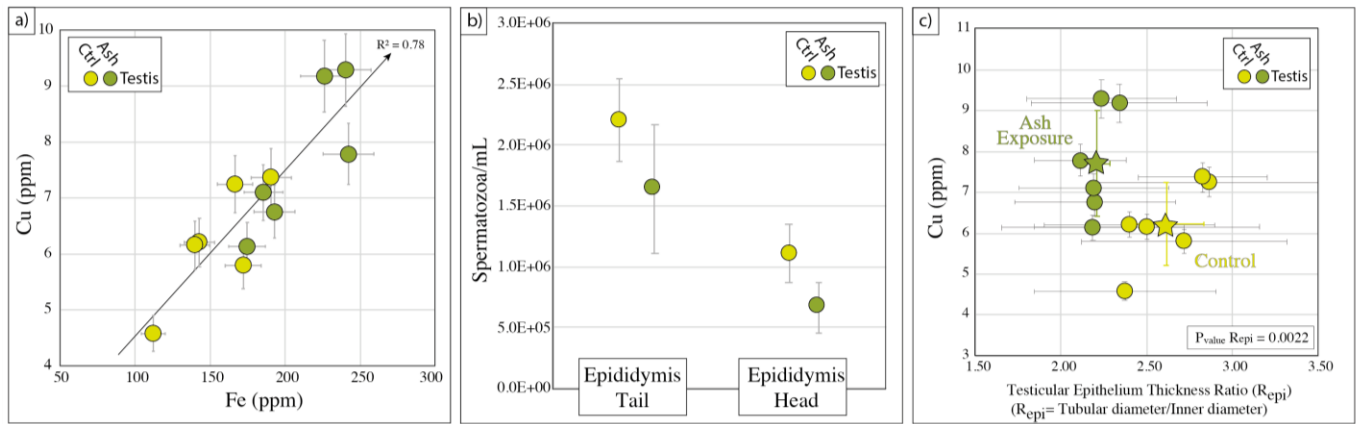


Figure 4: Volcanic ash-related metallomic and physiological deregulations in testes

After one month of exposure to metal-rich volcanic ash, mice present (a) testicular copper (Cu) and iron (Fe) accumulation (b) a decrease of the sperm count in the tail and the head of the epididymis and (c) a drop of the testicular epithelium thickness associated to copper increase. Light and dark points stand for control and exposed subjects, respectively. In the left corner diagram (a), for each datapoint, error bars represent 2sd. For the central diagram (b), error bars represent $1sd/\sqrt{n}$ with $n=6$ (i.e. 6 different samples per group from individual mice). Note that for each individual sample, data was obtained on the average of $n=3$ complete duplicate analyses. For the right corner diagram (c), error bars represent 2sd for Cu concentrations and 1sd for epithelium thickness obtained on the average of >20 seminiferous tubules per sample. Stars stand for the group average and for testicular epithelium thickness, the approximate p -value was determined by a two-sided non-parametric Mann-Whitney U-test implemented in MATLAB™.

807

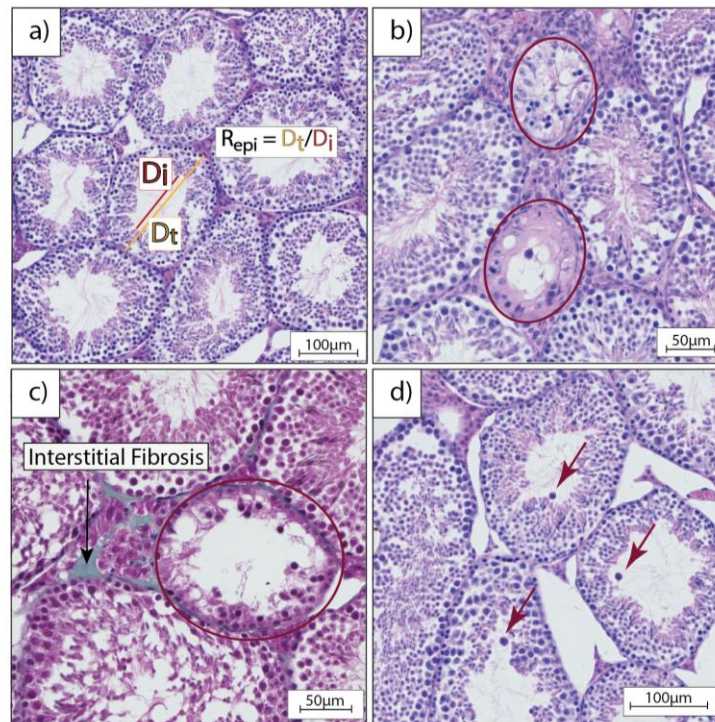


Figure 5: Histology of mice seminiferous tubules by Hematoxylin/Eosin (HE) and Masson's Trichrome (TM) staining

Representative micrographs of the testis of (a) control and (b,c and d) mice exposed to volcanic ash. The original magnification was $\times 20$. Mice exposed to volcanic ash present germinal epithelium degeneration and tubular vacuolation (b and c) highlighted by red rounded circle, sign of preliminary fibrosis (c) (highlighted by the black arrow and revealed by green coloration with TM staining) and abnormal amount of intratubular atypical germ cells (d) evidenced by the red arrows.

808

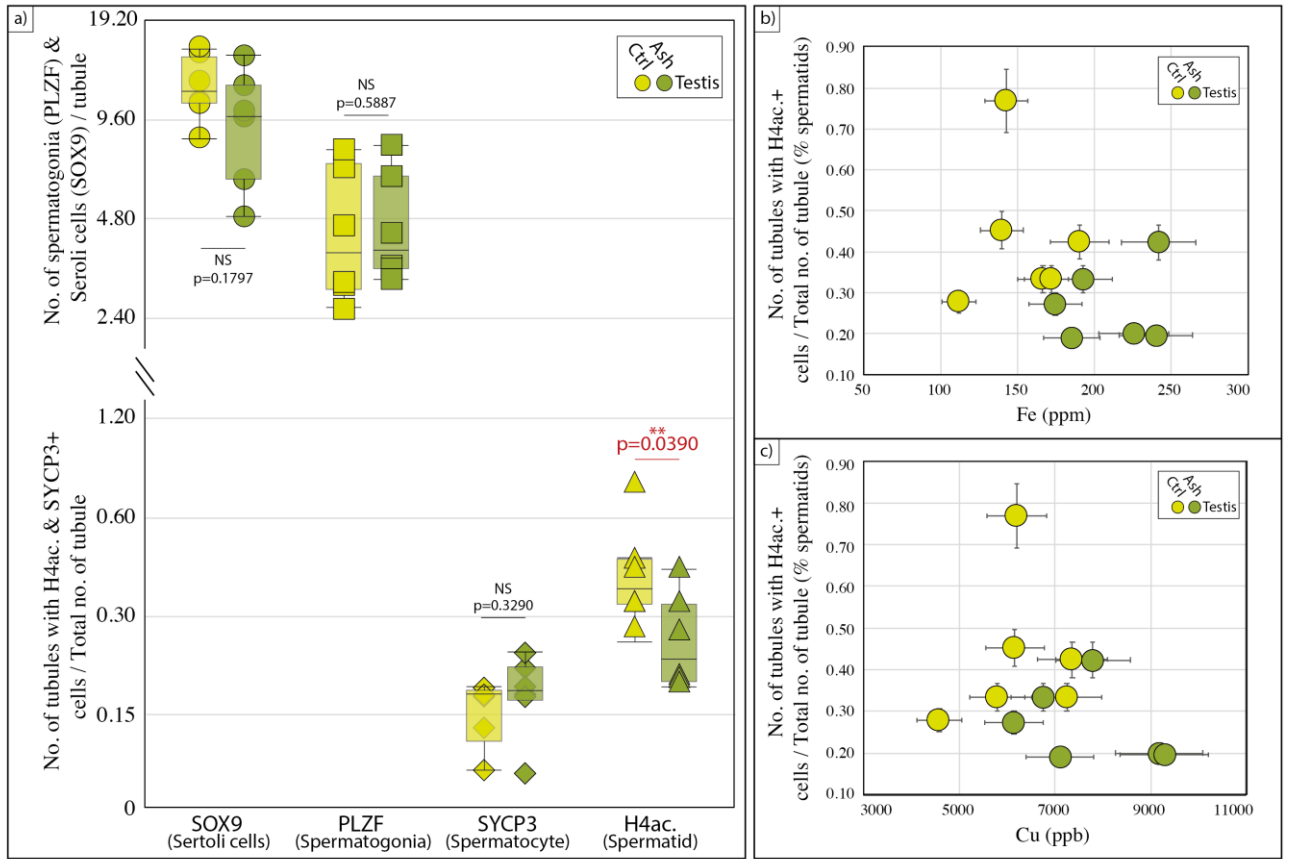


Figure 6: Immunohistochemical quantification of seminiferous tubules

(a) Number of normal seminiferous tubules of control and volcanic-ash exposed C57BL/6 males (n=6 per group). Statistical analysis: NS stand for non significant value, ** is for p<0.05 (two-sided non-parametric Mann-Whitney U-test implemented in MATLABM) (b) & (c) Correlation between the testicular Fe and Cu concentration and the number of acetyl H4+ tubules versus the total number of tubules (n>20). Error bars represent 2sd.

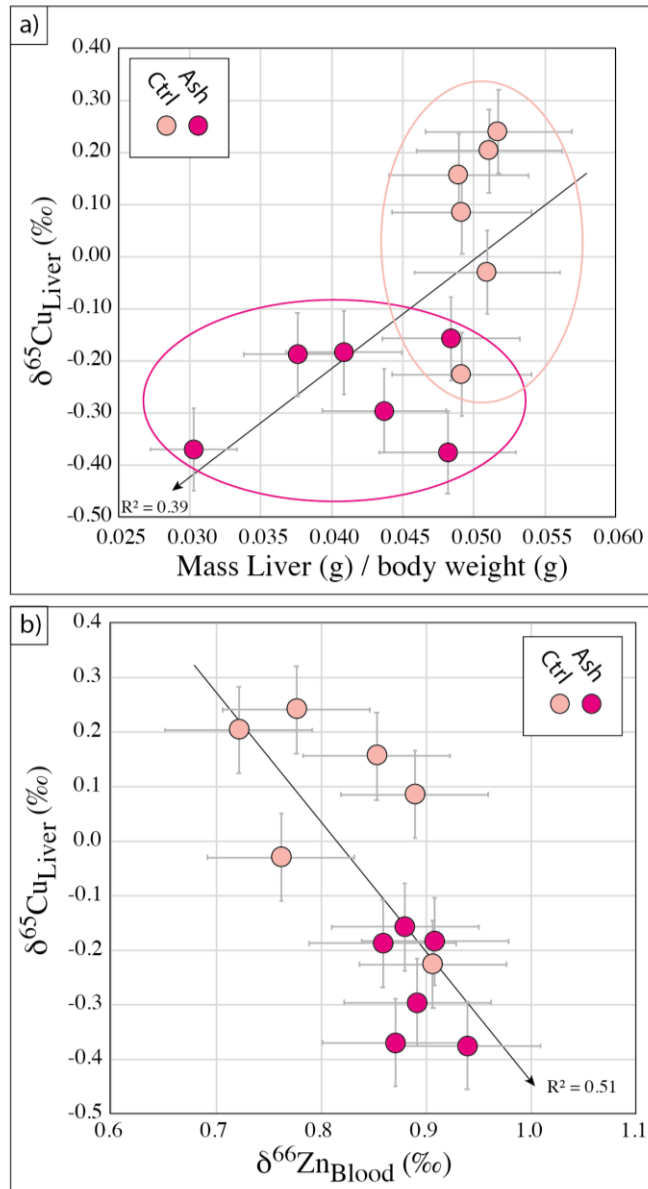
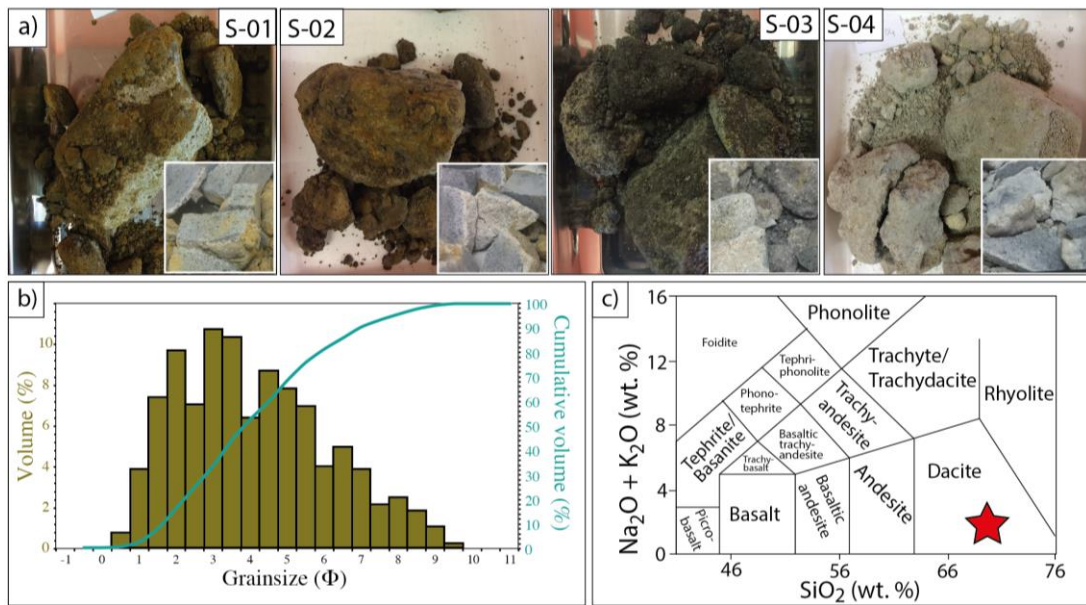


Figure 7: Volcanic ash-related isotopic and physiological deregulations in liver and blood mice

Mice exposed to volcanic ash present a significant decrease of the hepatic copper isotopic composition ($\delta^{65}\text{Cu}$) in association with (a) a liver mass loss and (b) a rise of the blood zinc isotopic composition ($\delta^{66}\text{Zn}$). Light and dark points stand for control and exposed subjects, respectively. For each value, analytical error bars represent 2sd.

812
813

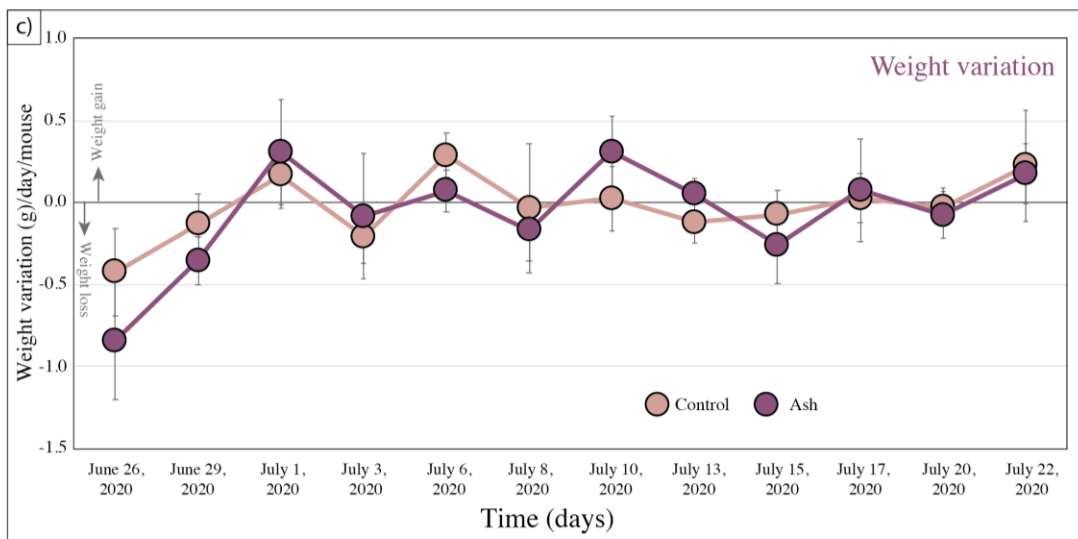
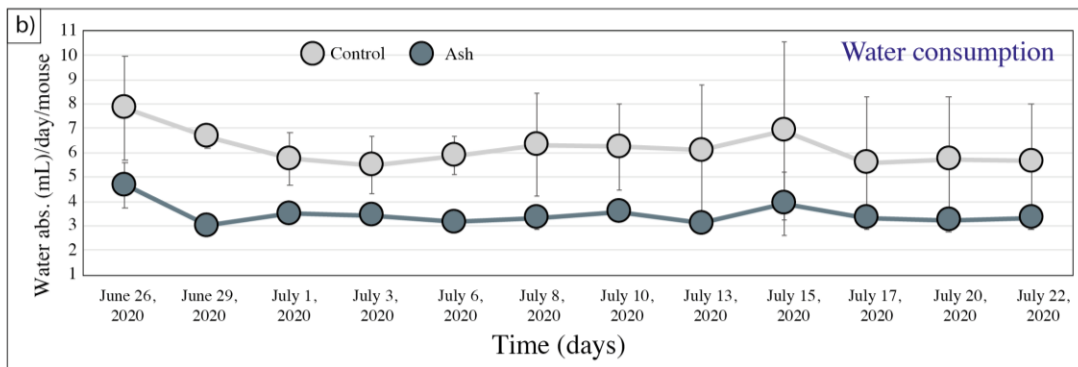
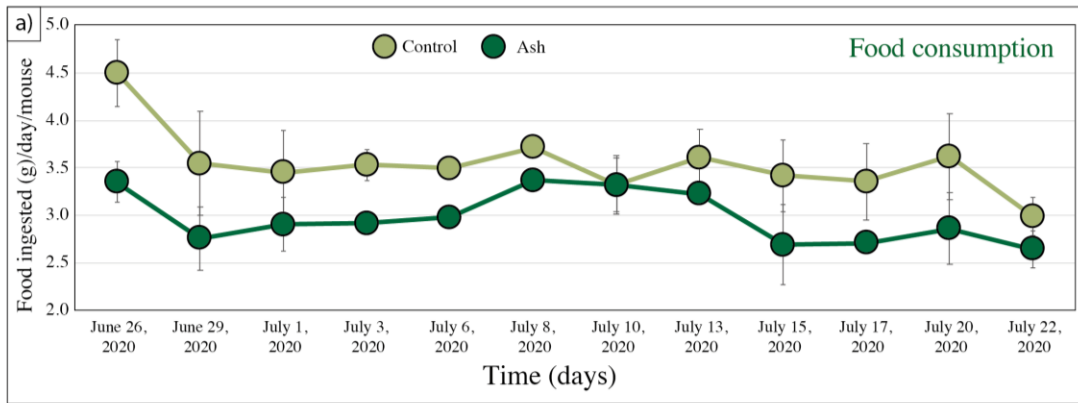
Supplementary Figures:



Supplementary Figure 1: Volcanic sample characterisation

(a) Visual aspect of the interior and the surface alteration of the four volcanic samples (S-01 to S-04) analyzed in this study, (b) Particle size distribution ($\Phi = -\log_2(d)$) with d the diameter of the particle in mm) of the *lab-crushed* volcanic ash sample determined by laser diffraction analyses using a Malvern Mastersizer® analyzer and (c) TAS diagram showing the chemical composition of the volcanic ash sample (red star) as a function of its silica (SiO_2) and alkaline ($\text{Na}_2\text{O}+\text{K}_2\text{O}$) content.

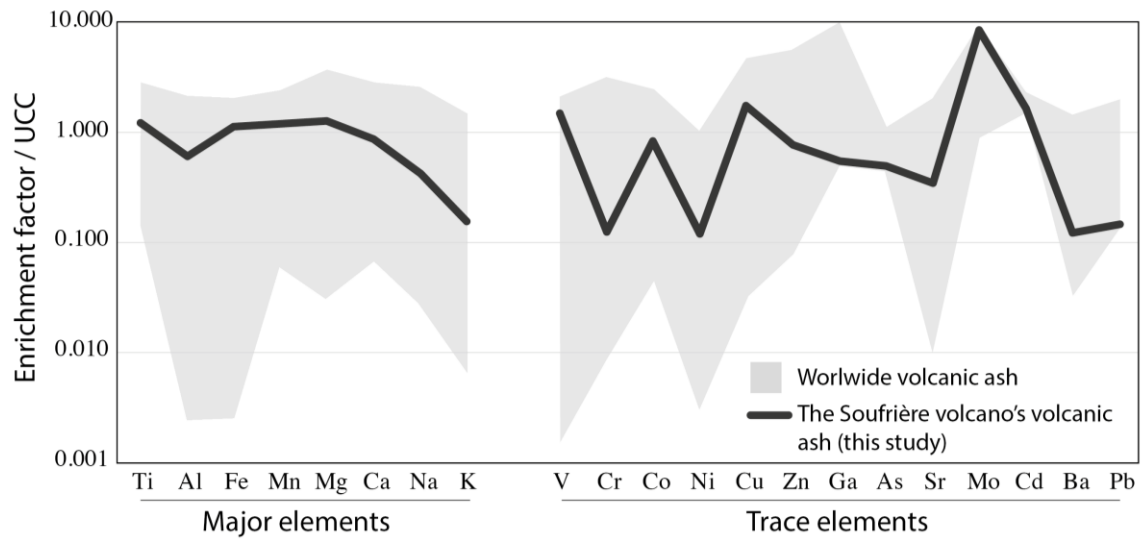
814



Supplementary Figure 2: Diet and weight variation over time exposure

Mice exposed over a month to volcanic ash are characterized by (a) Food and (b) Water consumption decrease but (c) no weight variation. Light and dark color point represent control and exposed subjects respectively. For each value, error bars represent 1sd obtained on the average of six data per group (i.e., n=6 mice per group)

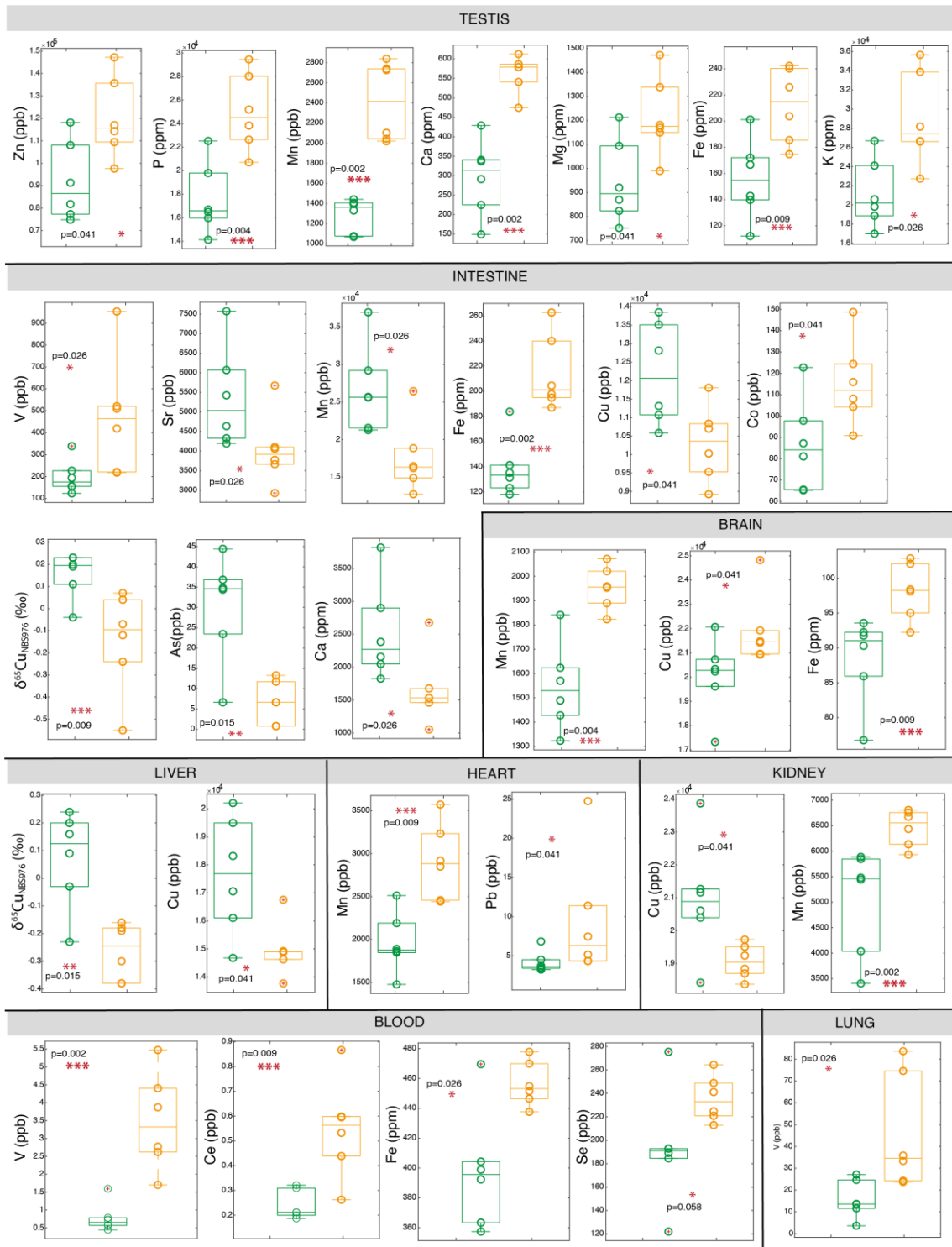
815
816
817
818
819



Supplementary Figure 3: Major and trace element patterns of the volcanic ash sample normalized to the upper continental crust (UCC)

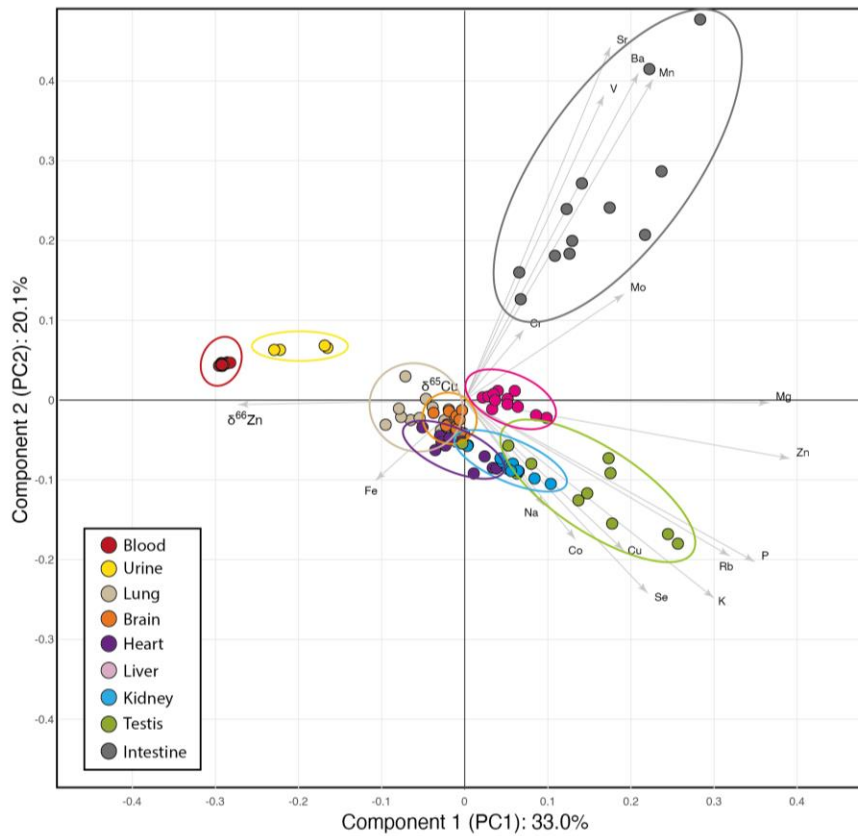
The black line stands for the Soufrière volcanic ash analysed in this study. The grey field represents the average of worlwide volcanic ash obtained on a data compilation from 16 volcanoes/country (Yasur/Vanuatu: Stewart et al., 2006, Cordon Caulle/Chile: Stewart et al., 2016; Eyjafjallajökull/Iceland: Gislason et al., 2011; El Chichón/Mexico: Varekamp et al., 1984; Sinabung/Indonesia: Kusmartini et al., 2017; Puna/Argentina: Ruggieri et al., 2010; Chaitén/Chile: Ruggieri et al., 2012; Shihan/Jordania: Ibrahim et al., 2014; Grímsvötn/Denmark: Lieke et al., 2013; Alpine Anthering/Austria: Huber et al., 2003; Tianchi volcano/China: Ma et al., 2019; Popocatépetl/Mexico: Shruti et al., 2018; Mt Etna/Italy: Toscano et al., 2008; Mt St Helens/USA: Taylor et al., 1980). The average values for the UCC are from Rudnick and Gao, 2014.

820
821
822
823
824



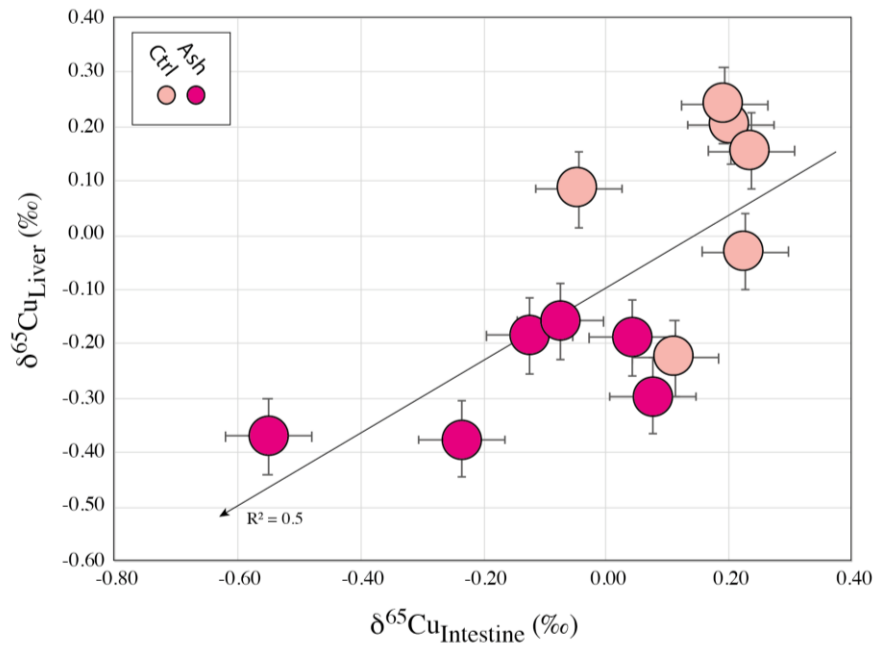
Supplementary Figure 4: Volcanic ash-related metallome deregulations in mice biological compartments

Green and yellow points stand for the control and the exposed subjects, respectively. For each diagram, the statistical p -value was determined between the control and the exposed group ($n=6$ per group and per reservoir) by a two-sided non-parametric Mann-Whitney U-test implemented in MATLAB™. Only significant p -value (<0.05) are shown with *, ** and *** standing for p -value lower than 0.05, 0.02 and 0.01 respectively. With only two points per group, no statistical processing could have been done on the urine reservoir.



Supplementary Figure 5: Principal Component Analysis (PCA) of the Results

The PCA allows the classification and the distinction of each mice body reservoirs (organs and body fluids) based on their metallome (i.e., major and trace element and copper, zinc isotopes compositions). In this diagram, all the samples from both the control and the exposed group are represented without any color distinction. The PCA variables include the chemical concentrations of 16 major and trace elements measured in 7 organs and 2 biological fluids of mice, as well as $\delta^{65}\text{Cu}$ and $\delta^{66}\text{Zn}$ values. Grey arrow are graphic representations of loading factors in the new PC1 vs. PC2 space. Each body reservoir is distinguishable by a specific color. All data were normalized, and samples with incomplete data were excluded. PCA was implemented in MATLAB™.



Supplementary Figure 6: Hepatic and intestinal copper isotopic compositions ($\delta^{65}\text{Cu}$)
 Mice exposed to volcanic ash present a significant decrease of the hepatic $\delta^{65}\text{Cu}$ in association with intestinal $\delta^{65}\text{Cu}$ drop. Light and dark points stand for control and exposed subjects, respectively. For each value, analytical error bars represent 2sd.

827
 828
 829
 830
 831
 832

Supplementary Tables:

Supplementary Table 1: Geological sampling location

Sample Name	Sampling date (day/hour)	Longitude	Latitude	Altitude (m)
		UTM coordinate (WGS84)		
S-04	2019-11-18 16:30:36	643041.2877	1774176.37	1453.79
S-03	2019-11-18 16:42:47	643050.5657	1774131.397	1443.32
S-02	2019-11-18 16:54:32	642961.1668	1774222.988	1454.19
S-01	2019-11-18 17:07:48	642955.7651	1774247.627	1442.91

833
 834
 835

Supplementary Table 3: Food ingested, water absorbed and weight variation over time exposure

Measurement Date	Food ingested (g) / day / mouse				Water absorbed (mL) / day / mouse				Weight variation (g) / day / mouse			
	Control Group (n=6)	1 σ (n=6)	Exposed group (n=6)	1 σ (n=6)	Control Group (n=6)	1 σ (n=6)	Exposed group (n=6)	1 σ (n=6)	Control Group (n=6)	1 σ (n=6)	Exposed group (n=6)	1 σ (n=6)
2020-06-26	4.5	0.4	3.4	0.2	7.8	2.1	4.7	0.9	-0.4	0.3	-0.8	0.4
2020-06-29	3.5	0.5	2.8	0.3	6.7	0.5	3.0	0.2	-0.1	0.2	-0.4	0.1
2020-07-01	3.5	0.4	2.9	0.3	5.8	1.1	3.5	0.2	0.2	0.2	0.3	0.3
2020-07-03	3.5	0.2	2.9	0.1	5.5	1.2	3.4	0.1	-0.2	0.2	-0.1	0.4
2020-07-06	3.5	0.0	3.0	0.0	5.9	0.8	3.2	0.4	0.3	0.1	0.1	0.1
2020-07-08	3.7	0.1	3.4	0.1	6.3	2.1	3.3	0.5	0.0	0.4	-0.2	0.2
2020-07-10	3.3	0.3	3.3	0.3	6.3	1.8	3.6	0.4	0.0	0.2	0.3	0.2
2020-07-13	3.6	0.3	3.2	0.1	6.1	2.7	3.1	0.3	-0.1	0.1	0.0	0.1
2020-07-15	3.4	0.4	2.7	0.4	6.9	3.7	3.9	1.3	-0.1	0.2	-0.3	0.2
2020-07-17	3.4	0.4	2.7	0.1	5.6	2.7	3.3	0.0	0.0	0.2	0.1	0.3
2020-07-20	3.6	0.5	2.9	0.4	5.7	2.6	3.2	0.5	0.0	0.1	-0.1	0.1
2020-07-22	3.0	0.2	2.6	0.2	5.7	2.4	3.3	0.5	0.2	0.3	0.2	0.2

837
838

Supplementary Table 4: Mass of the entire organ (wet weight i.e., before freeze-drying) normalised to body weight at sacrifice date

	Sample Name	Mass organ (g) / Body weight (g)				
TESTIS	T1	0.0058				
	T2	0.0059				
	T3	0.0062				
	T4	0.0056				
	T5	0.0046				
	T6	0.0069				
	T7	0.0067				
	T8	0.0048				
	T9	0.0062				
	T10	0.0067				
	T11	0.0065				
	T12	0.0068				
LUNG	Lu1	0.0065				
	Lu2	0.0048				
	Lu3	0.0052				
	Lu4	0.0047				
	Lu5	0.0064				
	Lu6	0.0044				
	Lu7	0.0050				
	Lu8	0.0052				
	Lu9	0.0048				
	Lu10	0.0064				
	Lu11	0.0045				
	Lu12	0.0053				
INTESTINE	I1	0.0370				
	I2	0.0322				
	I3	0.0241				
	I4	0.0315				
	I5	0.0287				
	I6	0.0263				
	I7	0.0316				
	I8	0.0272				
	I9	0.0304				
	I10	0.0311				
	I11	0.0275				
	I12	0.0246				
BRAIN	Br1	0.0132				
	Br2	0.0133				
	Br3	0.0132				
	Br4	0.0127				
	Br5	0.0138				
	Br6	0.0156				
	Br7	0.0146				
	Br8	0.0138				
	Br9	0.0149				
	Br10	0.0148				
	Br11	0.0139				
	Br12	0.0137				
LIVER	Liv1	0.0492				
	Liv2	0.0492				
	Liv3	0.0510				
	Liv4	0.0511				
	Liv5	0.0517				
	Liv6	0.0489				
	Liv7	0.0437				
	Liv8	0.0376				
	Liv9	0.0303				
	Liv10	0.0482				
	Liv11	0.0408				
	Liv12	0.0484				
HEART	H1	0.0055				
	H2	0.0056				
	H3	0.0060				
	H4	0.0054				
	H5	0.0052				
	H6	0.0049				
	H7	0.0042				
	H8	0.0051				
	H9	0.0054				
	H10	0.0045				
	H11	0.0042				
	H12	0.0046				
KIDNEY	K1	0.0102				
	K2	0.0108				
	K3	0.0119				
	K4	0.0118				
	K5	0.0116				
	K6	0.0120				
	K7	0.0117				
	K8	0.0110				
	K9	0.0132				
	K10	0.0124				
	K11	0.0101				
	K12	0.0099				

Table caption: Sample ID from 1 to 6 stand for control mice and from 7 to 12 for mice exposed to volcanic ash over one month

Supplementary Table 5: Spermatozoa count in the tail and the head of epididymis of C57BL/6 control (ID: 1 to 6) and exposed mice (ID: 7 to 12) to volcanic ash

	Mice ID	Sperm count / mL (n=3)	σ/Vn (n=3)	Average Sperm count / mL (n=6)	σ/Vn (n=6)
Epididymis Tail	1	2.1E+06	2.9E+05	2.21E+06	3.42E+05
	2	1.2E+06	1.6E+05		
	3	2.7E+06	8.4E+05		
	4	1.6E+06	2.0E+04		
	5	3.5E+06	9.6E+05		
	6	2.3E+06	0.0E+00		
Epididymis Tail	7	1.1E+06	3.7E+05	1.64E+06	5.32E+05
	8	1.1E+06	2.0E+04		
	9	3.6E+06	7.8E+05		
	10	6.3E+05	6.1E+04		
	11	4.8E+05	2.0E+04		
	12	3.0E+06	7.6E+05		
Epididymis Head	1	1.9E+06	6.9E+05	1.11E+06	2.36E+05
	2	5.5E+05	0.0E+00		
	3	1.6E+06	1.0E+05		
	4	5.0E+05	1.6E+05		
	5	8.3E+05	3.9E+05		
	6	1.3E+06	0.0E+00		
Epididymis Head	7	5.0E+05	2.0E+05	6.63E+05	2.07E+05
	8	2.0E+05	4.1E+04		
	9	4.3E+05	2.0E+04		
	10	6.5E+05	2.4E+05		
	11	1.7E+06	3.7E+05		
	12	5.5E+05	4.1E+04		

840
841

Supplementary Table 6: Testicular epithelium thickness ratio & Immunohistochemical quantification

Sample Name	Testicular epithelium thickness		Immunohistochemical quantification			
	R_{epi} (Testicular Epithelium Thickness Ratio)	1σ (n=20)	No. of acetyl-Histone H4+ tubule/total tubule	No. of SYCP3+ tubule/total tubule	No. of PLZF+ cells/tubule (n>20)	No. of SOX9+ cells/tubule (n>20)
T1	2.44	0.65	0.77	0.17	2.55	10.72
T2	2.78	0.74	0.45	0.18	2.98	10.59
T3	3.17	0.77	0.33	0.08	6.82	15.09
T4	2.82	0.44	0.42	-	7.69	12.40
T5	2.57	0.40	0.33	0.17	3.05	15.82
T6	2.43	0.38	0.28	0.12	4.54	8.33
T7	2.07	0.47	0.20	0.17	7.93	9.73
T8	2.10	0.27	0.42	0.21	3.42	12.05
T9	1.98	0.23	0.33	0.19	3.35	6.28
T10	2.17	0.36	0.20	0.24	6.39	10.13
T11	2.07	0.39	0.27	0.05	3.11	4.81
T12	2.05	0.33	0.19	0.17	4.32	14.80

Table caption: Sample from T1 to T6 stand for control mice and from T7 to T12 for mice exposed to volcanic ash over one month

842
843

Supplementary Table Z: Major, trace element concentrations and Cu/Zn isotopic composition of geological sample and reference material

Sample Name	Major elements (wt %)											Trace elements (ppm)											Isotopic composition																				
	SiO ₂	Al ₂ O ₃	Fe ₂ O ₃ tot	MgO	CaO	Na ₂ O	K ₂ O	TiO ₂	MnO	P ₂ O ₅	LOI	Total	Li	V	Cr	Co	Ni	Cu	Zn	Ga	As	Rb	Sr	Mo	Cd	Ba	La	Ce	Pr	Nd	Sm	Eu	Gd	Tb	Dy	Ho	Er	Tm	Yb	Lu	Pb	$\delta^{65}\text{Cu}_{\text{VSMO}}$	$\delta^{66}\text{Zn}_{\text{NIST}}$
Volcanic Ash (m-s)	69.25	9.35	6.40	3.18	3.15	2.35	0.44	0.79	0.12	0.03	5.56	99.64	<LO	146.01	11.57	14.44	5.52	49.70	51.88	9.71	2.40	10.84	111.71	9.52	0.15	86.25	1.64	10.00	1.43	6.51	1.81	0.47	2.70	0.39	2.61	0.59	1.81	0.28	1.87	0.33	2.68	-0.52	0.38
2sd	0.69	0.20	0.08	0.28	0.15	0.20	0.02	0.04	0.00	0.02	-	-	<LO	49.31	0.70	1.00	0.33	3.15	2.63	0.55	0.12	0.65	4.55	0.46	0.03	5.53	0.11	0.32	0.05	0.19	0.04	0.02	0.15	0.04	0.15	0.07	0.18	0.05	0.20	0.05	0.06	0.11	0.02
BHW02 (m-s)	49.75	14.30	12.31	7.57	11.78	2.62	0.52	2.80	0.18	0.30	-	100.14	5.73	315.09	28.112	43.36	116.78	128.47	96.90	21.95	0.97	9.02	376.51	4.08	0.18	126.04	15.04	35.83	5.20	24.29	5.98	2.02	6.28	0.95	5.21	0.96	2.91	0.32	1.95	0.28	1.43	0.06	0.32
2sd	0.50	3.21	0.58	1.32	1.18	1.42	0.01	0.11	0.03	0.12	-	0.51	0.57	32.00	18.59	5.86	16.06	15.46	25.74	4.64	0.46	1.94	24.95	2.21	0.12	6.97	0.95	2.00	0.44	2.18	0.33	0.12	0.48	0.10	0.39	0.06	0.22	0.01	0.17	0.02	0.11	0.04	0.01
Certified value BHW02	49.90	13.50	12.30	7.23	11.40	2.22	0.52	2.73	0.17	0.27	-	100.24	5.00	317.00	280.00	45.00	119.00	127.00	103.00	21.70	0.70	9.80	389.00	4.07	0.15	130.00	15.20	37.53	5.34	25.00	6.20	2.04	6.30	0.94	5.28	1.04	2.91	0.33	1.99	0.28	1.65	0.09	0.27
2sd	1.20	0.40	0.40	0.24	0.40	0.16	0.02	0.08	0.01	0.04	-	-	0.09	22.00	38.00	6.00	14.00	14.00	12.00	1.80	0.11	2.00	46.00	0.16	0.05	25.00	2.00	2.00	0.03	3.60	0.80	0.01	0.38	0.01	0.03	0.08	0.01	0.00	0.03	0.02	0.04	0.06	0.05

Table caption: n stands for complete duplicate analysis; <LO stands for lower limit of detection calculated following IUPAC guidelines for each element; 1 sd = xbi and standard deviation of the number of counts measured in bla

“-” stand for not measured sample

Figure 1

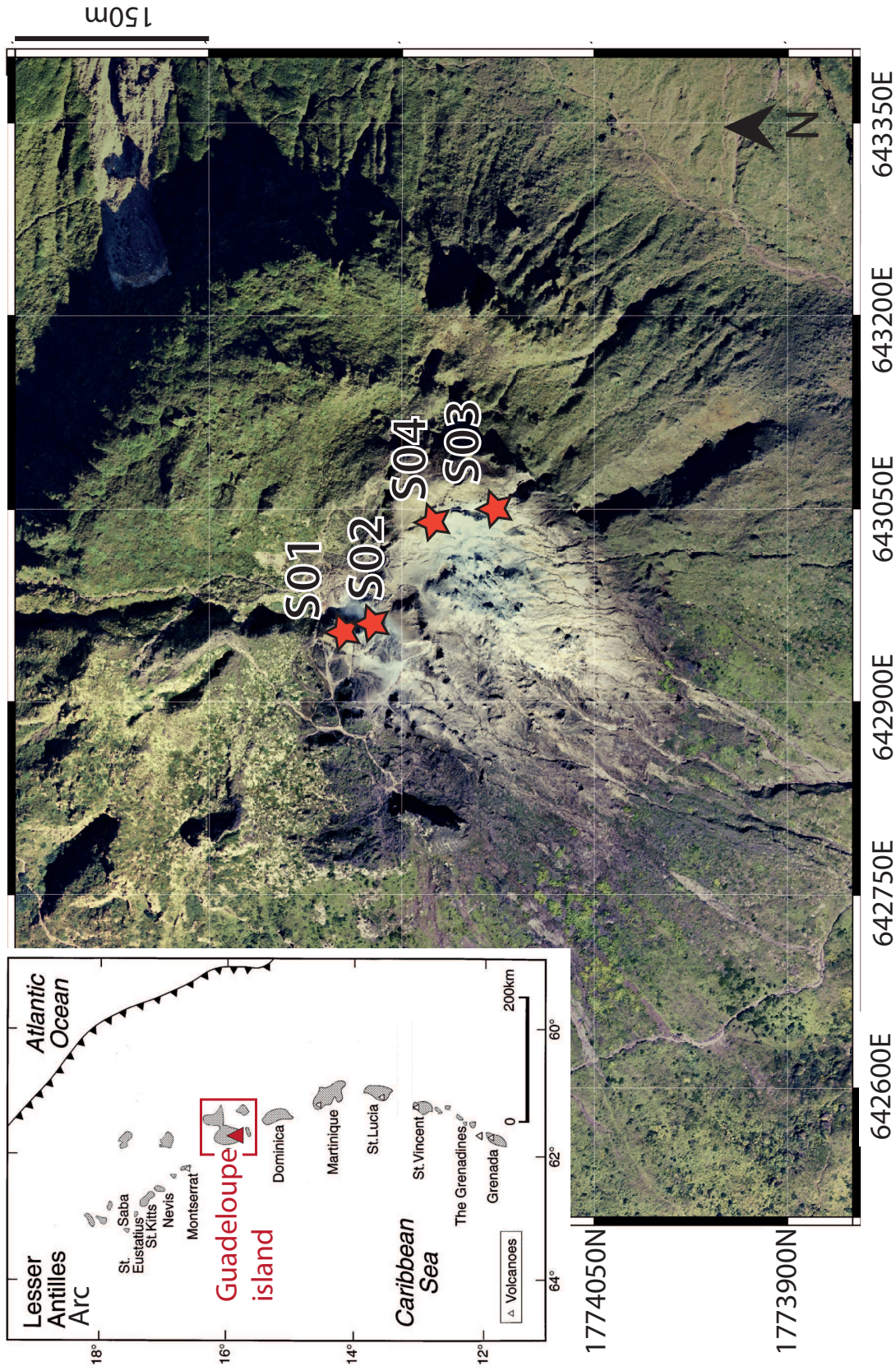


Figure 1: Location map of the studied area

Map of the Soufrière volcano located in the Guadeloupe island (Basse-Terre) of the Lesser Antilles arc (UTM coordinates). The red triangle indicate the location of the Soufrière volcano and the red stars indicate the sampling locations of the rocks from the volcanic dome (S01 to S04) used to reproduce «artificial» volcanic ash later exposed to mice in this study. S01 and S02 were collected on the «Tarissan» site while S03 and S04 are from the «Cratère Sud» site.

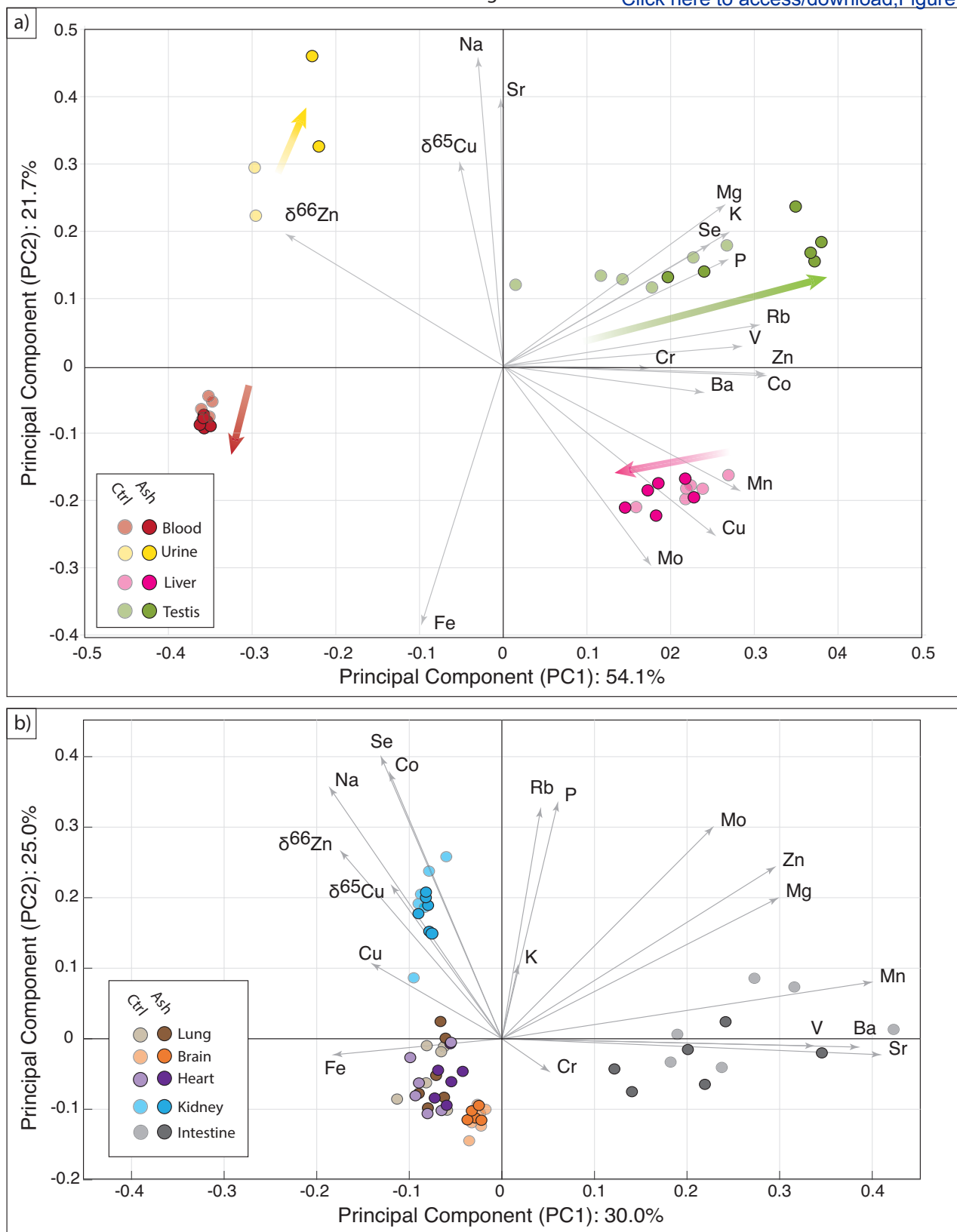


Figure 2. Principal Component Analysis (PCA) of the Results

The PCA allows (a) the identification of organs (i.e. testis and liver) and body fluids (i.e. blood and urine) preferentially affected by metallome deregulation (i.e. metallome difference between control and exposed subjects) due to volcanic ash exposure from (b) those that are less (i.e. no metallome difference between control and exposed subjects). In this study, the variables include the chemical concentrations of 16 major and trace elements measured in 7 organs and 2 biological fluids of mice, as well as $\delta^{65}\text{Cu}$ and $\delta^{66}\text{Zn}$ values. Grey arrows are graphic representations of loading factors in the new PC1 vs. PC2 space. The coordinates of each sample in the new PC1 vs. PC2 space (i.e. sample scores) are shown by circles. Transparency and solid points stand for control and exposed subjects, respectively. All data were normalized, and samples with incomplete data were excluded. PCA was implemented in MATLAB™.

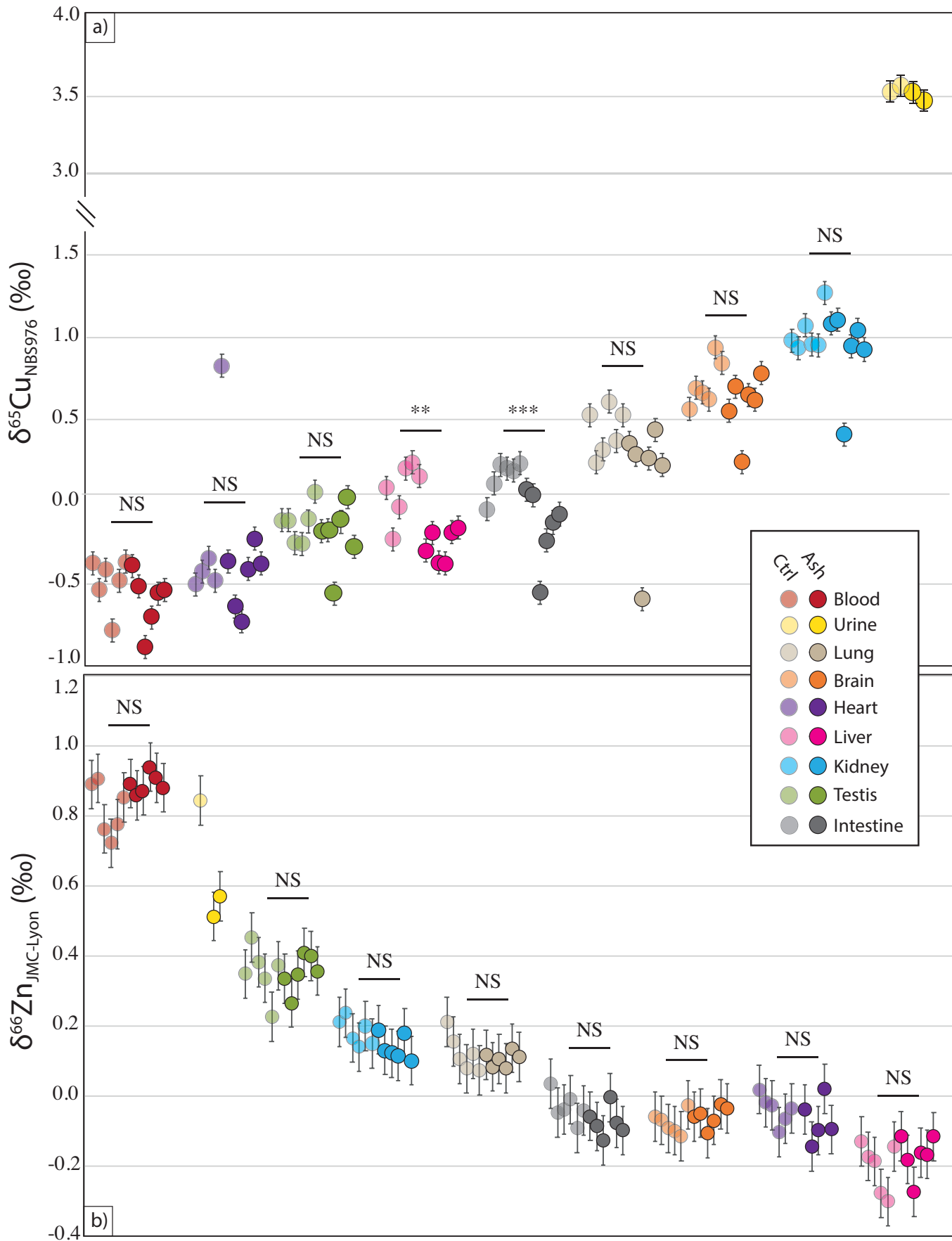


Figure 4

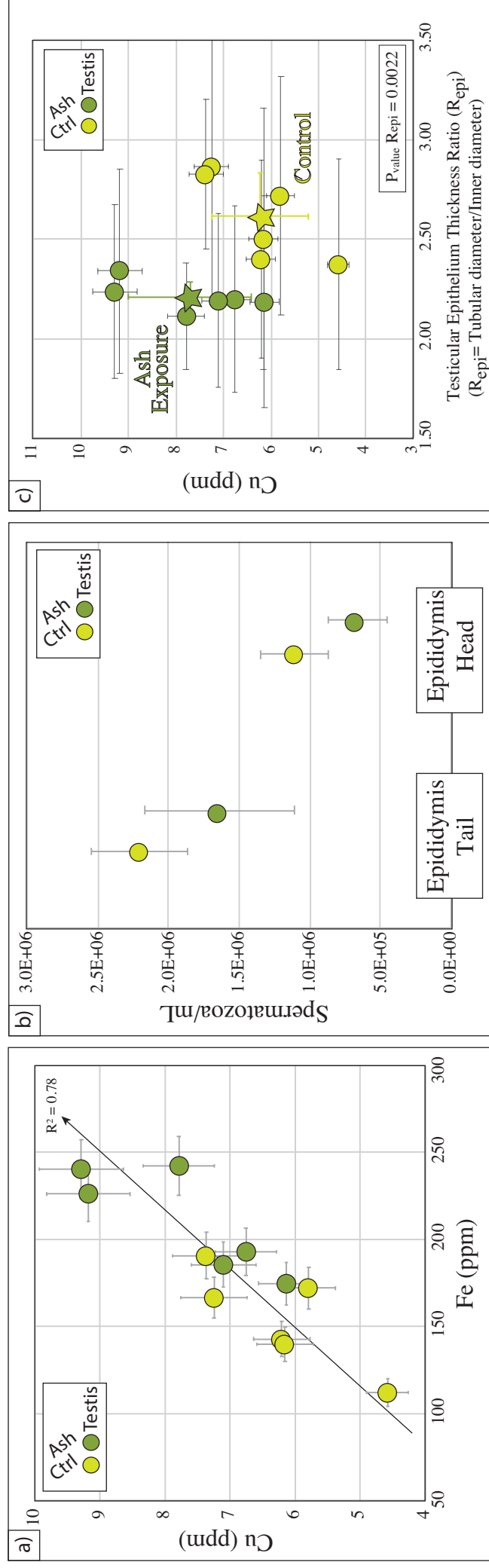


Figure 4: Volcanic ash-related metallomic and physiological deregulations in testes

After one month of exposure to metal-rich volcanic ash, mice present (a) testicular copper (Cu) and iron (Fe) accumulation

(b) a decrease of the sperm count in the tail and the head of the epididymis and (c) a drop of the testicular epithelium thickness associated to copper increase. Light and dark points stand for control and exposed subjects, respectively. In the left corner diagram (a), for each datapoint, error bars represent 2sd. For the central diagram (b), error bars represent 1sd/ \sqrt{n} with $n=6$ (i.e. 6 different samples per group from individual mice). Note that for each individual sample, data was obtained on the average of $n=3$ complete duplicate analyses. For the right corner diagram (c), error bars represent 2sd for Cu concentrations and 1sd for epithelium thickness obtained on the average of >20 seminiferous tubules per sample. Stars stand for the group average and for testicular epithelium thickness, the approximate p -value was determined by a two-sided non-parametric Mann-Whitney U-test implemented in MATLAB™.

Figure 5

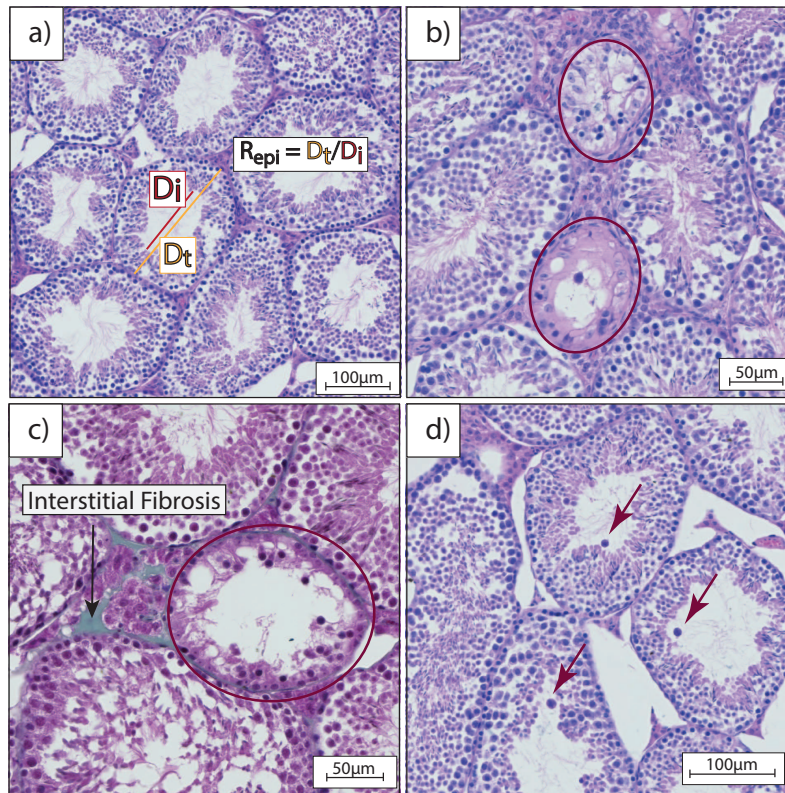


Figure 5: Histology of mice seminiferous tubules by Hematoxylin/Eosin (HE) and Masson's Trichrome (TM) staining

Representative micrographs of the testis of (a) control and (b,c and d) mice exposed to volcanic ash. The original magnification was x20. Mice exposed to volcanic ash present germinal epithelium degeneration and tubular vacuolation (b and c) highlighted by red rounded circle, sign of preliminary fibrosis (c) (highlighted by the black arrow and revealed by green coloration with TM staining) and abnormal amount of intratubular atypical germ cells (d) evidenced by the red arrows.

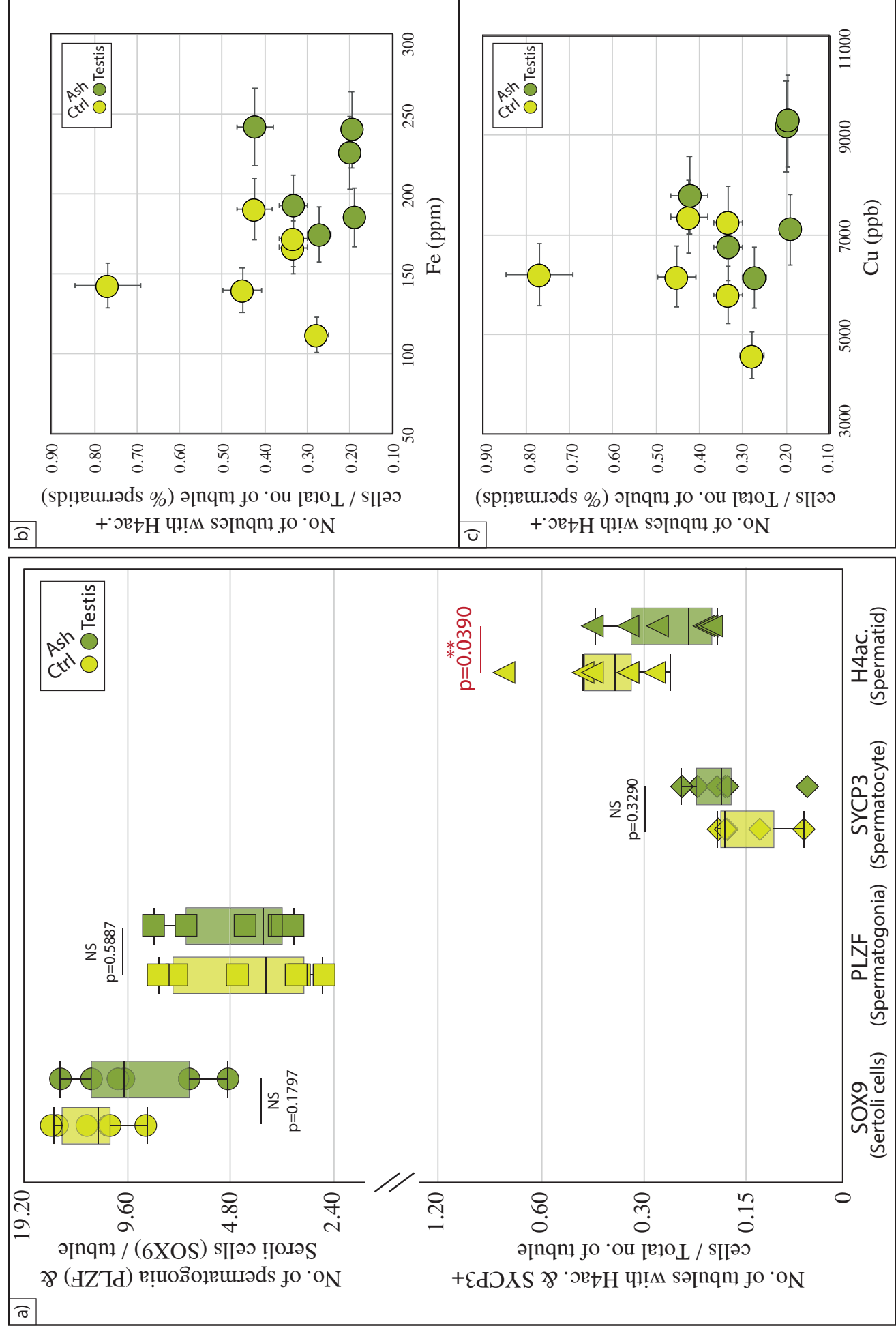


Figure 6: Immunohistochemical quantification of seminiferous tubules

(a) Number of normal seminiferous tubules of control and volcanic-ash exposed C57BL/6 males (n=6 per group). Statistical analysis: NS stand for non significant value, ** is for p<0.05 (two-sided non-parametric Mann-Whitney U-test implemented in MATLAB™) (b) & (c) Correlation between the testicular Fe and Cu concentration and the number of acetyl H4+ tubules versus the total number of tubules (n>20). Error bars represent 2sd.

Figure 7

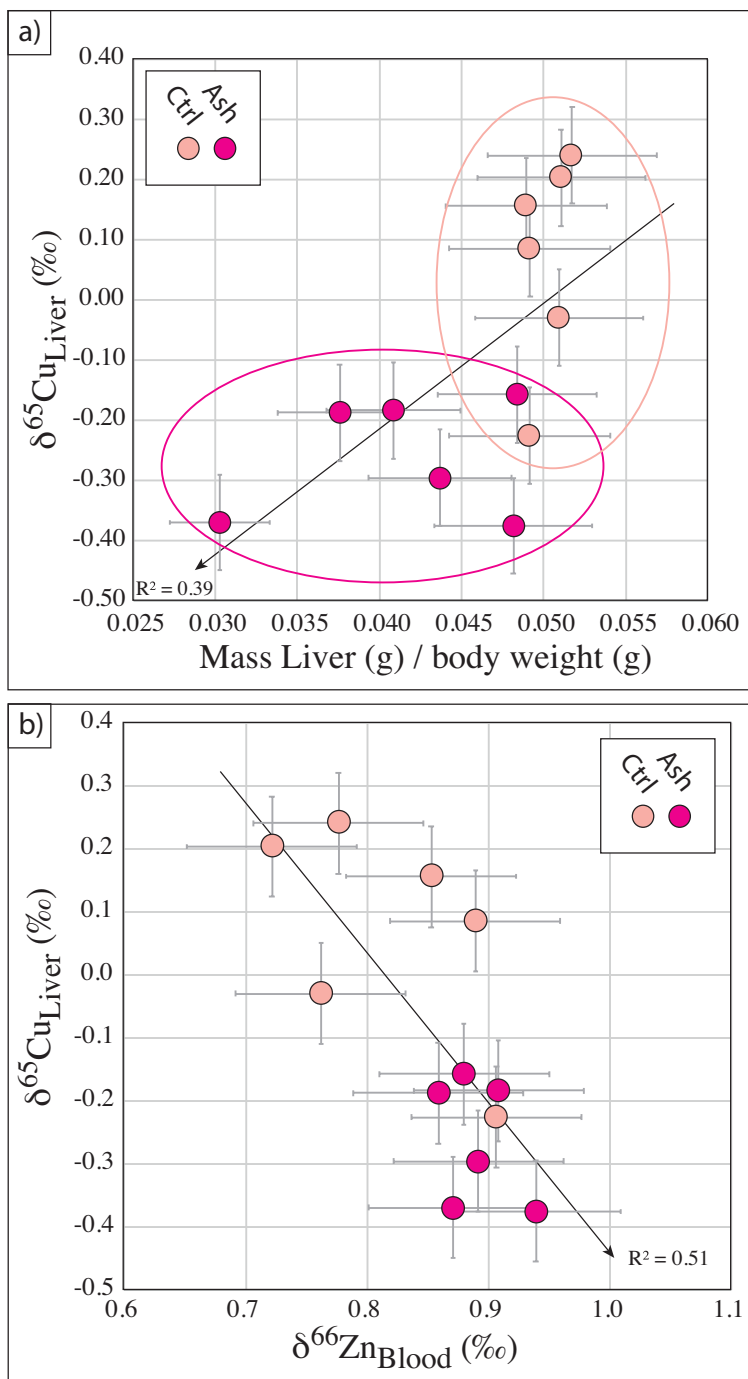


Figure 7: Volcanic ash-related isotopic and physiological deregulations in liver and blood mice

Mice exposed to volcanic ash present a significant decrease of the hepatic copper isotopic composition ($\delta^{65}\text{Cu}$) in association with (a) a liver mass loss and (b) a rise of the blood zinc isotopic composition ($\delta^{66}\text{Zn}$). Light and dark points stand for control and exposed subjects, respectively. For each value, analytical error bars represent 2sd.



Click here to access/download
Supplementary Material
Supp Table2.xlsx





Click here to access/download
Supplementary Material
Supp Table 1.xlsx





Click here to access/download
Supplementary Material
Supp Table3.xlsx





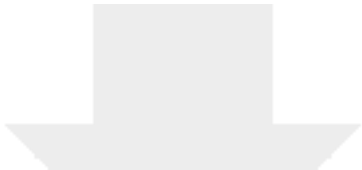
Click here to access/download
Supplementary Material
Supp Table4.xlsx



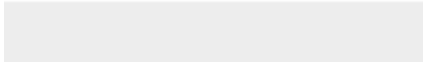


Click here to access/download
Supplementary Material
Supp Table5.xlsx





Click here to access/download
Supplementary Material
Supp Table6.xlsx





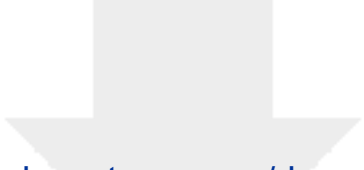
Click here to access/download
Supplementary Material
Supp Table7.xlsx






Click here to access/download
Supplementary Material
Supp Figure1.eps





Click here to access/download
Supplementary Material
Supp Figure2.eps





Click here to access/download
Supplementary Material
Supp Figure3.eps





Click here to access/download
Supplementary Material
Supp Figure4.eps





Click here to access/download
Supplementary Material
Supp Figure5.eps





Click here to access/download
Supplementary Material
Supp Figure6.eps



Declaration of interests

The authors declare that they have no known competing financial interests or personal relationships that could have appeared to influence the work reported in this paper.

The authors declare the following financial interests/personal relationships which may be considered as potential competing interests:

Sample CRediT author statement

Sauzéat Lucie: Conceptualization, Methodology, Software, Validation, Investigation, Writing – Original draft, Review & Editing, Visualization, Supervision, Project administration, Funding acquisition;

Julia Eychenne: Writing – Review & Editing, Methodology, Investigation

Lucia Gurioli: Resources, Writing – Review & Editing

Maud Boyet: Supervision, Writing – Review & Editing

David Jessop: Resources, Writing – Review & Editing

Roberto Moretti: Resources, Writing – Review & Editing

Mélusine Monroe: Investigation

Hélène Holota: Investigation

Claude Beaudoin: Writing – Review & Editing

David Volle: Supervision, Methodology, Investigation, Writing – Review & Editing